



Water Resources Research®

RESEARCH ARTICLE

10.1029/2022WR033731

Key Points:

- Plant access to groundwater is often ignored in global evaporation estimates, yet it can be crucial during dry conditions
- A new, conceptual approach to incorporate groundwater-sourced evaporation in existing global, satellite-based models is presented
- Considering groundwater affects the dynamics of evaporation in 22% of the continental surface and increases global land evaporation by 0.5%

Correspondence to:

P. Hulsman,
Petra.Hulsman@ugent.be

Citation:

Hulsman, P., Keune, J., Koppa, A., Schellekens, J., & Miralles, D. G. (2023). Incorporating plant access to groundwater in existing global, satellite-based evaporation estimates. *Water Resources Research*, 59, e2022WR033731. <https://doi.org/10.1029/2022WR033731>

Received 21 SEP 2022

Accepted 20 JUL 2023

Incorporating Plant Access to Groundwater in Existing Global, Satellite-Based Evaporation Estimates

P. Hulsman¹ , J. Keune¹ , A. Koppa¹ , J. Schellekens², and D. G. Miralles¹ 

¹Hydro-Climate Extremes Lab (H-CEL), Ghent University, Ghent, Belgium, ²Planet, Haarlem, The Netherlands

Abstract Groundwater is an important water source for evaporation, especially during dry conditions. Despite this recognition, plant access to groundwater is often neglected in global evaporation models. This study proposes a new, conceptual approach to incorporate plant access to groundwater in existing global evaporation models, and analyses the groundwater contribution to evaporation globally. To this end, the Global Land Evaporation Amsterdam Model (GLEAM) is used. The new GLEAM-Hydro model relies on the linear reservoir assumption for modeling groundwater flow, and introduces a transpiration partitioning approach to estimate groundwater contributions. Model estimates are validated globally against field observations of evaporation, soil moisture, discharge and groundwater level for the time period 2015–2021, and compared to a regional groundwater model. Representing groundwater access influences evaporation in 22% of the continental surface. Globally averaged, evaporation increases by 2.5 mm year^{-1} (0.5% of terrestrial evaporation), but locally, evaporation can increase up to $245.2 \text{ mm year}^{-1}$ (149.7%). The groundwater contribution to transpiration is highest for tall vegetation under dry conditions due to more frequent groundwater access. The temporal dynamics of the simulated evaporation improve across 75% of the stations where groundwater is a relevant water source. The skill of the model for variables such as soil moisture and runoff remains similar to GLEAM v3. The proposed approach enables a more realistic process representation of evaporation under water-limited conditions in satellite-data driven models such as GLEAM, and sets the ground to assimilate satellite gravimetry data in the future.

Plain Language Summary Groundwater can be a crucial source of water for plants: plants that have access to groundwater through their root system are more likely to survive periods of rainfall scarcity. However, many (satellite-based) models neglect this water source and assume plants only depend on the unsaturated-zone soil moisture. This assumption results in underestimated evaporation values during dry conditions, when groundwater may become the main (or even the only) source of water. In this study, we propose a new approach to improve evaporation estimates under water-stressed conditions by incorporating groundwater in an existing global, satellite-based evaporation model, and we assess the impact of groundwater on evaporation globally. The impact of this modification on the model's accuracy and on the resulting evaporation is evaluated. Representing groundwater increases the evaporation globally by 2.5 mm year^{-1} (0.5%) with much higher increases in certain regions.

1. Introduction

Land evaporation couples the energy and water cycles, cooling the surface (K. Trenberth et al., 2009) and supplying 40% of terrestrial precipitation (Oki & Kanae, 2006; K. E. Trenberth et al., 2007; van der Ent et al., 2010). Accurate evaporation estimates are crucial, not only for improved understanding of the water and energy cycles (e.g., Koppa et al., 2021), but also for specific applications, such as irrigation planning, drought prediction, monitoring ecosystem health, and estimating water availability for societies (Fisher et al., 2017; Konapala et al., 2020; Vicente-Serrano et al., 2010). Unfortunately, in situ observations of evaporation are often point-based and limited in space and time, making it difficult to obtain accurate estimates over large, heterogeneous regions and long time periods. As a result, evaporation is often calculated based on meteorological and surface data using either dedicated algorithms, or more complex land surface and hydrological models, in which evaporation uncertainties will propagate to both atmospheric and hydrological variables such as temperature and runoff.

During the past two decades, multiple satellite-based evaporation algorithms have been developed. These algorithms enable the estimation of evaporation globally, including poorly gauged regions, and thus facilitate global-scale applications (Kalma et al., 2008; K. Zhang et al., 2016; J. Zhang et al., 2020). Satellite-based

© 2023. The Authors.

This is an open access article under the terms of the [Creative Commons Attribution License](#), which permits use, distribution and reproduction in any medium, provided the original work is properly cited.

evaporation algorithms often aim to close the energy balance (Bastiaanssen et al., 1998; Mallick et al., 2014; Su, 2002), employ empirical methods based on in situ observations (Jung et al., 2009), or compute stress indicators to constrain potential evaporation (Fisher et al., 2008; Miralles et al., 2011). Some of these evaporation products also use soil moisture estimates to assess plant water availability for transpiration (e.g., Loew et al., 2016; Miralles et al., 2011). Similarly, many hydrological (e.g., Bieger et al., 2017; Samaniego et al., 2010) and land surface models (e.g., Blyth et al., 2021; Clark et al., 2015) estimate evaporation as a function of soil moisture. However, these models often assume plants only have access to the water stored in the unsaturated zone which is solely replenished from the surface, that is, they assume groundwater is not a relevant water source for transpiration. But in many regions of the world plant roots have access to groundwater (e.g., Evaristo & McDonnell, 2017; Fan, 2015; Kollet & Maxwell, 2008; Maxwell & Condon, 2016; Miguez-Macho & Fan, 2021; Taylor et al., 2013). Miguez-Macho and Fan (2021) use inverse modeling and isotope observations to illustrate that 32% of land evaporation in the Mediterranean originates from groundwater during dry months, whereas the globally-averaged contribution is limited to 1%. Barbeta and Peñuelas (2017) use global isotope data to show that groundwater uptakes constitute on average 49% of evaporation in dry seasons and 28% in wet seasons.

Many studies have explored the added value of incorporating groundwater interactions in existing models. One popular avenue has been the coupling of land surface or hydrological models to a groundwater model (e.g., Amanambu et al., 2020; de Graaf et al., 2017; Kuffour et al., 2020; Maxwell & Miller, 2005; Sulis et al., 2017; Tian et al., 2012). These models typically aim to improve the simulation of soil moisture by introducing interactions with groundwater, which then indirectly influences evaporation estimates. While two-way coupling with groundwater models allows for a more accurate representation of the subsurface, the increased data and computational requirements challenge the application at large scales (Condon et al., 2021; Gleeson et al., 2021) such that it is not routinely applied in global models. To overcome this challenge, several studies propose adding a single groundwater layer that interacts with the soil moisture in the unsaturated zone, assuming that lateral groundwater flow is insignificant at the chosen spatio-temporal resolution (e.g., Lam et al., 2011; Niu et al., 2007; Sutanudjaja et al., 2018; Yeh & Eltahir, 2005). Other approaches include the estimation of groundwater-sourced evaporation directly, for example, as a function of the soil moisture (Liu et al., 2015; Liu & Luo, 2012) or the fraction of roots accessing groundwater (Laio et al., 2009; Orellana et al., 2012).

Modeling studies that simulate groundwater-surface interactions typically detect higher groundwater uptake by plant roots under dry conditions (Balugani et al., 2017; Lam et al., 2011; Maxwell & Condon, 2016; Miguez-Macho & Fan, 2021). This is also confirmed with a field experiment by Tfwala et al. (2021) who show that under dry conditions, total transpiration decreases while its groundwater contribution increases. Barbeta and Peñuelas (2017) find that the groundwater uptake is independent of the depth to the groundwater table in saturated soils, which is possibly due to the increased water-uptake efficiency of roots (Orellana et al., 2012). This is also concluded by Beyer et al. (2018) who state that “*even if the fraction of roots reaching the water table is small, the efficiency of tap roots can be hundreds of times larger than roots in drier soil and large amounts of water can be transported.*” However, uncertainty regarding the impact of groundwater on evaporation remains large and stems, among others, from the considered root depth that determines whether plants have access to the aquifer, or soil properties that influence the hydraulic conductivity and the corresponding groundwater level (Fan et al., 2017; Keune et al., 2016; Sulis et al., 2019).

In this study, we propose a novel, conceptual approach to incorporate plant access to groundwater in large-scale models, and analyze the impact of groundwater on evaporation globally. The proposed approach is based on two concepts: (a) a linear reservoir for the groundwater flow (e.g., Fenicia et al., 2006; Gao et al., 2014; Sutanudjaja et al., 2018), and (b) a partitioning of transpiration into contributions from the unsaturated zone and groundwater that reflects an increased groundwater uptake during dry conditions (Liu et al., 2015; Liu & Luo, 2012). The approach is incorporated in the satellite-based Global Land Evaporation Amsterdam Model (GLEAM), and its impact on land evaporation estimates is evaluated. The structure of the paper is as follows: Section 2 describes the new GLEAM-Hydro model. Sections 3 and 4 describe the input data and validation strategy. Results on the validation and the simulated impact of groundwater on global evaporation are presented and discussed in Sections 5 and 6, respectively, before conclusions are drawn in Section 7.

2. Methods

This study assesses the effect of groundwater on global evaporation by representing plant access to groundwater in a satellite-based evaporation model. For this purpose, a linear reservoir approach for the groundwater flow is used and a groundwater contribution factor, that describes the fraction of evaporation sourced from groundwater, is introduced (Section 2.1.4). Here, we incorporate the proposed approach in GLEAM, creating a new version of the model, hereafter referred to as GLEAM-Hydro. The effect of groundwater on evaporation is assessed globally by comparing GLEAM-Hydro to the baseline GLEAM v3.

2.1. GLEAM-Hydro

2.1.1. Baseline GLEAM v3

The baseline model for GLEAM-Hydro is GLEAM (Miralles et al., 2011) on its current version 3 (v3) (Martens et al., 2017). GLEAM v3 estimates the total evaporation as the sum of interception loss, transpiration, bare soil evaporation, open-water evaporation, and sublimation. Transpiration (E_t) is estimated by constraining potential evaporation (E_p) with a stress factor S_t (i.e., $E_t = S_t \cdot E_p$) which is a function of soil moisture and vegetation optical depth (VOD) to account for changes in phenology. The VOD indicates how much the vegetation attenuates the propagation of microwaves; a dense canopy attenuates microwaves more resulting in higher VOD values (Frappart et al., 2020; Martens et al., 2017). Similarly, bare soil evaporation (E_b) is estimated using a stress factor which is a function of the soil moisture only (Martens et al., 2017). Potential evaporation is estimated with the Priestley and Taylor (1972) equation. Within each grid cell, the following four land cover types are distinguished: tall vegetation, short vegetation, bare soil, and open water bodies. The root zone is divided into three soil layers (0–0.1 m, 0.1–1 m, 1–2.5 m) depending on the land cover fraction, that is, tall vegetation has three soil layers, short vegetation two, and bare soil a single layer. Below the bottom soil layer, the water content is assumed to be at field capacity at all times, and a free drainage approach is applied. Thus, in GLEAM v3, E_t and E_b depend only on the energy demand (i.e., E_p) and water availability in each soil layer (i.e., w)—see Martens et al. (2017) for more information.

2.1.2. Groundwater Reservoir Water Balance

In GLEAM-Hydro, the groundwater system is represented by a single reservoir with only one inflow (i.e., recharge) and multiple fluxes leaving the system (i.e., groundwater flow, evaporation and overland flow), assuming lateral groundwater flow is insignificant. The groundwater reservoir is implemented at the grid cell level, that is, the groundwater level is assumed to be the same for all land cover classes, and comprises the entire soil column. The implementation further allows differentiating between the water volumes stored in the saturated zone in and/or below the three soil layers (S_s), and the groundwater levels (GWL).

The water balance for S_s is estimated with

$$\frac{dS_s}{dt} = Q_r - Q_s - E_{GW} - Q_{OF} \quad (1)$$

with Q_r recharge into saturated zone [mm day^{-1}], Q_s groundwater flow [mm day^{-1}], E_{GW} groundwater-sourced evaporation [mm day^{-1}], and Q_{OF} overland flow [mm day^{-1}]. The change in GWL is linearly related to the change in S_s (Healy & Cook, 2002; Lv et al., 2021):

$$\frac{dGWL}{dt} = \frac{1}{\theta_y} \cdot \frac{dS_s}{dt} \quad (2)$$

$$\theta_y = \theta_{\text{por}} - \theta_{\text{fc}} \quad (3)$$

with θ_y specific yield [$\text{m}^3 \text{m}^{-3}$], θ_{por} soil porosity [$\text{m}^3 \text{m}^{-3}$], and θ_{fc} field capacity [$\text{m}^3 \text{m}^{-3}$].

2.1.3. Recharge, Groundwater Flow and Overland Flow

The recharge is assumed to be equal to the drainage leaving the bottom soil layer across all land cover classes. Here, groundwater flow is defined as the amount of water leaving a grid cell from the saturated layer and is

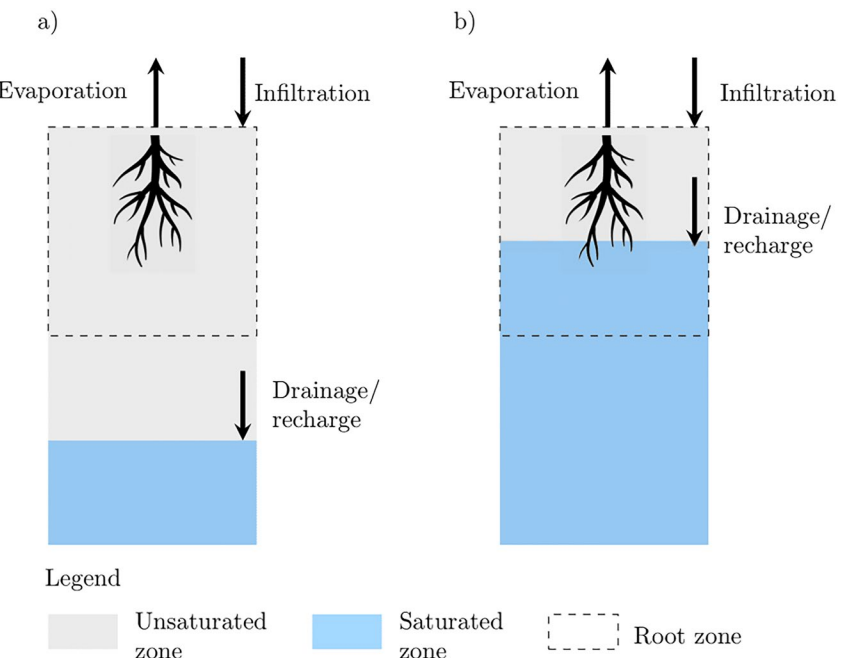


Figure 1. Scheme of plant water sources available for evaporation. (a) Deep groundwater: water in the root zone originates only from infiltration (e.g., rainwater, irrigation, snow melt etc.), (b) Shallow groundwater: water in the root zone originates from infiltration and groundwater.

estimated with the linear reservoir assumption, as commonly used in (global) hydrological models (e.g., Gao et al., 2014; Samaniego et al., 2010; Sutanudjaja et al., 2018):

$$Q_s = \max(0, S_s) \cdot K_s \quad (4)$$

with the recession constant K_s [day^{-1}]. When plant roots have access to groundwater, groundwater-sourced evaporation is greater than zero and estimated with Equations 6 and 9 (see Section 2.1.4). Overland flow occurs when GWL exceed the surface level:

$$Q_{OF} = \frac{\max(0, GWL \cdot \theta_y)}{\Delta t} \quad (5)$$

with Δt the time step which is equal to 1 day [day]. Note that the land surface is used as a reference for the groundwater level, which is defined as negative below the surface and positive above the surface.

2.1.4. Groundwater-Sourced Evaporation

When plants do not have access to groundwater, then all the water stored in the root zone comes from the surface through infiltration (see Figure 1a). However, when plants have access to groundwater, then water for evaporation originates from both infiltration ($E_{t,\text{nonGW}}$) and groundwater ($E_{t,\text{GW}}$, see Figure 1b). We assume that plants extract water first from the groundwater system, considering that water is more easily accessible there, before plants extract water from soil moisture stored above the water table. Note that the maximum rooting depths considered here are 0.1–2.5 m depending on the land cover class (see Section 2.1.1), and that plants cannot access the groundwater system beyond that depth in GLEAM-Hydro. In this study, we assume groundwater contributions may be substantial, even if the flow path from roots to leaves is long and the root density decreases with root depth. This assumption is in agreement with the following findings of previous studies: Deep taproots are thicker and have a high hydraulic conductivity that allows them to extract substantial amounts of water (Beyer et al., 2018; Orellana et al., 2012), making the groundwater uptake independent of the water table depth in saturated soils if plants have access to the groundwater system (Barbeta & Peñuelas, 2017), see also Section 1.

To distinguish between the uptake of groundwater and infiltrated water for transpiration, the groundwater contribution fraction (f_{GW} , [-]) is introduced as (similar to Liu & Luo, 2012):

$$f_{GW} = \min\left(1, \max\left(0, \frac{1}{l_{sat,max}} \cdot \sum_{l=1}^{l_{sat,max}} \frac{\theta_{l,flc} - w_l}{\theta_{l,flc} - \theta_{l,crt}}\right)\right) \quad (6)$$

with l soil layer number [-], $l_{sat,max}$ maximum number of soil layers in the root zone affected by groundwater [-], θ_{flc} field capacity [$m^3 m^{-3}$], w soil moisture [$m^3 m^{-3}$], and θ_{crt} critical soil moisture [$m^3 m^{-3}$]. The relative contribution of groundwater to transpiration is defined such that it is highest under dry conditions and lowest under wet conditions; that is, $f_{GW} = 1$ if $w \leq \theta_{crt}$ (dry soil) and $f_{GW} = 0$ if $w \geq \theta_{flc}$ (wet soil). If the groundwater affects multiple soil layers, then the fraction is averaged over the affected layers.

Transpiration is divided into $E_{t,GW}$ and $E_{t,nonGW}$ by incorporating f_{GW} into the evaporative stress factor:

$$S_t = f_{GW} \cdot S_{t,GW} + (1 - f_{GW}) \cdot S_{t,nonGW} \quad (7)$$

with S_t combined stress factor [-], $S_{t,GW}$ groundwater stress factor [-], and $S_{t,nonGW}$ non-groundwater stress factor [-]. By definition, $S_{t,GW} = 1$ since there is no stress in the saturated zone. Analogous to GLEAM v3, $S_{t,nonGW}$ is a function of soil moisture in the unsaturated zone (Martens et al., 2017).

Transpiration E_t [mm day^{-1}] is then calculated as

$$E_t = f_{GW} \cdot S_{t,GW} \cdot E_p + (1 - f_{GW}) \cdot S_{t,nonGW} \cdot E_p \quad (8)$$

with

$$E_{t,GW} = f_{GW} \cdot S_{t,GW} \cdot E_p \quad (9)$$

the transpiration that is sourced from groundwater [mm day^{-1}], and

$$E_{t,nonGW} = (1 - f_{GW}) \cdot S_{t,nonGW} \cdot E_p \quad (10)$$

the transpiration sourced from soil moisture in the unsaturated zone [mm day^{-1}].

This approach is applied for all land cover fractions individually, that is, for tall vegetation, short vegetation and bare soil. The latter is included to represent water evaporating from shallow groundwater directly without root extraction (Balugani et al., 2017). The aggregated groundwater-sourced evaporation (E_{GW}) is then used in the water balance equation (Equation 1). With this approach, the total stress factor S_t cannot exceed 1, meaning that the total transpiration is always equal to or below potential evaporation. In addition, we assume that there is unlimited groundwater available for E_{GW} , that is, it is not possible at any point in time that plants have access to the groundwater system yet there is no groundwater available anymore. This assumption is simulated by estimating E_{GW} independently from S_s and hence by allowing E_{GW} to (occasionally) surpass the water volume stored in the groundwater reservoir, resulting in negative S_s values and GWL lower than the initial condition (see Section 2.2). In that case, there is no groundwater flow until the reservoir is refilled and S_s values are positive again (see Equation 4). This approach enables simulating the above mentioned assumption of an unlimited groundwater source available to plants while dealing with uncertainties in the initial conditions. Similar approaches have been applied in previous studies to simulate inter-basin groundwater flow (Hrachowitz et al., 2014). Furthermore, the two water sources available for evaporation in the root zone (infiltrated water and groundwater) are treated separately for simplicity. In other words, groundwater does not directly influence the unsaturated-zone soil moisture at or below the groundwater level, which allows for retaining the original GLEAM model structure. Nevertheless, this approach indirectly mimics the interaction between the unsaturated and saturated zone: With shallow GWL, the water content in the unsaturated zone becomes comparatively higher, as plants partly extract water from the groundwater instead of extracting only from the unsaturated zone.

2.2. Experiments Set-Up

GLEAM v3 and GLEAM-Hydro are run on a daily timescale at 0.25° resolution for the time period 2015–2021. Global analyses cover all land regions within 90°N–90°S and 180°E–180°W, whereas analyses for The Netherlands

cover the region 3°E–7.5°E and 50.5°N–54°N. In GLEAM-Hydro, initial conditions for *GWL* are based on the global water table depth from Fan et al. (2013) using the monthly mean values for January. Initial conditions for S_s are obtained through a spin-up, in which the model is run over the full period (2015–2021). The spin-up starts with long-term mean values for S_s , which is estimated with the water balance equation (Equation 1) assuming $\frac{dS_s}{dt} \approx 0$, zero groundwater-sourced evaporation and overland flow, applying Equation 4 for Q_s , and using recharge (Q_r) from GLEAM v3. Initial conditions for S_s to run GLEAM-Hydro are then based on the median S_s of January from the spin-up period.

3. Input Data

Satellite observations and reanalysis datasets are used as input. Air temperature is obtained from Atmospheric Infrared Sounder (AIRS) level 3 version 7.0 (Aumann et al., 2003). Net radiation and shortwave outgoing radiation are obtained from Clouds and the Earth's Radiant Energy System (CERES) Edition 4.1 (Wielicki et al., 1996). Precipitation data are obtained from the Multi-Source Weighted-Ensemble Precipitation version 2.8 (Beck et al., 2019). Snow water equivalent is based on GLOBSNOW v2.0 observations (Takala et al., 2011). Vegetation optical depth (VOD) is based on the Vegetation Optical Depth Climate Archive (VODCA, Moesinger et al., 2020). Soil properties are based on the data set Global Gridded Soil Characteristics produced by the International Satellite Land-Surface Climatology Project (ISLSCP, Scholes & Brown de Colstoun, 2011). Finally, land cover class fractions are derived from MOD44B version 6 Vegetation Continuous Fields (VCF, DiMiceli et al., 2015) by classifying all vegetation with a height of more (less) than 2 m as tall (short) vegetation. All observations are available globally and, if needed, interpolated bi-linearly to 0.25° resolution. These observations are used in both GLEAM v3 and GLEAM-Hydro consistently. In addition, GLEAM-Hydro includes recession constant data which are derived globally by Sutanudjaja et al. (2018) for the PCRaster GLOBal Water Balance model (PCR-GLOBWB). Furthermore, global water table depth observations according to Fan et al. (2013) are employed for the initial conditions as mentioned in Section 2.2.

4. Validation

GLEAM-Hydro is validated regionally over The Netherlands, where a reliable groundwater model and abundant in situ groundwater level observations are available, and globally using in situ observations of evaporation, soil moisture, discharge and *GWL*.

4.1. In Situ Observations

Global in situ observations with respect to evaporation, soil moisture, discharge and groundwater level are collected for the study period 2015–2021 from 10,951 sites. These observations are obtained from multiple platforms including AmeriFLUX, European Fluxes Database Cluster, FLUXNET-CH4, Global Runoff Data Center (GRDC), Integrated Carbon Observation System, International Groundwater Resources Assessment Center, and International Soil Moisture Network. See Table A1 for more information regarding observation type, number of sites per source, website links and references. These observations include not only variables directly used for validation, but also additional variables used, for example, to filter rain and snow days (i.e., precipitation, air temperature, snow depth, net radiation, surface heat flux and ground heat flux)—see below. For The Netherlands, the above-mentioned global databases provide data to validate evaporation and soil moisture. In addition, groundwater level observations at 2750 sites are available from the *Data en Informatie van de Nederlandse Ondergrond* (DINO) database.

In situ observations are pre-processed to remove outliers (values smaller or larger than the 1st or 99th percentile, respectively), duplicates, and daily observations with low-quality flag or coverage (<25%) at sub-daily scale where available. When validating evaporation, rain days (>0 mm day⁻¹) and stations with a poor energy balance closure are removed ($\frac{R_n - G - H}{LE} > 0.2$ with R_n net radiation, G ground heat flux, H surface heat flux, and LE latent heat flux). Evaporation is calculated from latent heat flux observations using air temperature data. When validating with respect to soil moisture, days with snowfall (>10 mm) or low temperature (<0°C) are removed. GLEAM-based soil moisture estimates are linearly interpolated to the depth of the observation. Sites with less than 365 observation points within the study period are removed. In case of gaps in the in situ observations used for the filtering procedure—that is, gaps in precipitation, snow or temperature data at the station—GLEAM

forcing data are used too. For the validation of runoff, stations with a temporal coverage of less than 75% are removed. In addition, discharge stations are removed when the corresponding gridded basin area at 0.25° resolution deviates substantially from the actual area as provided by GRDC (i.e., $| \frac{A_{\text{gridded}} - A_{\text{actual}}}{A_{\text{actual}}} | > 0.2$). Also, stations with a basin area smaller than 2,500 km² are not considered. Further, nested river basins are avoided by favoring downstream stations. Similar approaches for in situ data pre-processing have been applied in previous studies (Martens et al., 2017, 2020). Appendix Figure A1 visualizes all the stations available for validation after pre-processing.

4.2. Regional Validation: The Netherlands

Regional simulations of GLEAM v3 and GLEAM-Hydro for The Netherlands are validated using in situ data from 4 eddy-covariance, 22 soil moisture, and 1,714 groundwater level sites. See Section 4.1 for more information on the in situ observations used.

To assess the accuracy of the groundwater level estimates of GLEAM-Hydro, GWL from the groundwater model LHM version 4.1 (*Landelijk Hydrologisch Model*, <https://www.nhi.nu/nl/index.php/modellen/lhm/>) are used as a reference. LHM v4.1 uses MODFLOW (Langevin et al., 2017) for the saturated zone, metamodel Soil Water Atmosphere Plant for the unsaturated zone, World Food Studies for the plant growth simulation, and a distribution model for the water allocation (De Lange et al., 2014; Janssen et al., 2020). Note that this model does not consider feedbacks of evaporation on GWL. LHM-based groundwater level estimates are also validated against the same 1,714 groundwater level sites. As LHM simulations are only available until 2018, groundwater level validations over The Netherlands are done for the time period 2015–2018. The remaining variables are validated over the entire study period (2015–2021), depending on in situ data availability.

4.3. Global Validation

Global simulations of GLEAM v3 and GLEAM-Hydro are validated for the time period 2015–2021 using 100 eddy-covariance, 3,422 soil moisture, 97 discharge, and 1,329 groundwater level sites (Figure A1 in the Appendix). See Section 4.1 for more information on the in situ observations used.

4.4. Performance Metrics

Evaporation, soil moisture and GWL are validated by comparing observations and simulated time series from the respective grid cells where the stations are located. For this purpose, the following performance metrics are used: Spearman correlation coefficient (R), root mean square error ($RMSE$), and Kling-Gupta efficiency (KGE , Gupta et al., 2009). R ranges between -1 and 1 , $RMSE$ between 0 and ∞ , and KGE between $-\infty$ and 1 . A “perfect” performance is represented by $R = 1$, $RMSE = 0$ and $KGE = 1$. If the reference level of groundwater observations is unknown, performance metrics are estimated using groundwater level anomalies, that is, the observed and estimated data are subtracted by their mean using identical observation days.

Runoff from GLEAM is estimated based on the long-term water balance, assuming storage changes are insignificant compared to the magnitude of the fluxes over the simulation period, that is,

$$\bar{Q} = \bar{P} - \bar{E} \quad (11)$$

with \bar{Q} , \bar{P} and \bar{E} the long-term mean runoff, precipitation and evaporation, respectively. Runoff estimates are compared to discharge observations and their accuracy is evaluated with the mean difference ($MD = \bar{Q}_{\text{GLEAM}} - \bar{Q}_{\text{In situ}}$) and the percentage bias ($PBIAS = \frac{|\bar{Q}_{\text{GLEAM}} - \bar{Q}_{\text{In situ}}|}{\bar{Q}_{\text{In situ}}} \cdot 100\%$).

Table 1

Median Statistics for The Netherlands for Different Variables and Global Land Evaporation Amsterdam Model (GLEAM) Versions

Median values		GLEAM-v3	GLEAM-Hydro	LHM	Unit
Evaporation	R	0.90	0.90	n/a	–
	RMSE	0.85	0.85	n/a	mm day ⁻¹
	KGE	0.78	0.79	n/a	–
Soil moisture	R	0.74	0.74	n/a	–
	RMSE	7.69	7.94	n/a	%
	KGE	0.49	0.49	n/a	–
Groundwater	R	n/a	0.78	0.79	–
	RMSE	n/a	0.98	0.73	m
	KGE	n/a	-0.18	0.02	–

Note. Performance metrics include correlation (*R*), root mean square error (RMSE), and Kling-Gupta Efficiency (KGE).

5. Results

5.1. GLEAM-Hydro Validation

5.1.1. Regional Validation: The Netherlands

5.1.1.1. Evaporation

In The Netherlands and the near surroundings, evaporation is represented well by the reference model, GLEAM v3, with a median correlation of $R_{\text{median}} = 0.90$. The other performance metrics agree with the skill indicated by the correlation, with $\text{RMSE}_{\text{median}} = 0.85 \text{ mm day}^{-1}$ and $\text{KGE}_{\text{median}} = 0.78$ for GLEAM v3. Incorporating plant access to groundwater with GLEAM-Hydro does not affect these performance metrics and retains the median accuracy of the simulations (Table 1 and Figure 2). However, this assessment is based on only four eddy-covariance stations of which only one station (at Cabauw, 51.97°N and 4.93°E) is located in a region with shallow GWL (above -2.5 m). In addition, this station is located in a region that is primarily energy-limited, as any other station in The Netherlands. During the simulation period, 94% of the days at Cabauw show no or only little water limitation, that is, $E_p - E < 0.5 \text{ mm day}^{-1}$, which results in a small evaporation increase from 617.2 mm year⁻¹ (GLEAM v3) to 630.4 mm year⁻¹ (GLEAM-Hydro). Hence, over The Netherlands, groundwater barely affects the magnitude of transpiration.

5.1.1.2. Soil Moisture

The soil moisture is represented reasonably well by the reference model GLEAM v3 with a median correlation of $R_{\text{median}} = 0.74$. The remaining performance metrics are $\text{RMSE}_{\text{median}} = 7.69\%$ and $\text{KGE}_{\text{median}} = 0.49$ for GLEAM v3 (Table 1). Incorporating plant access to groundwater with GLEAM-Hydro does not affect the skill of the simulated soil moisture over The Netherlands (Table 1 and Figure 2c). This assessment is based on 22 sites, yet only 1 site is located in a region with shallow GWL (in Bergambacht near Cabauw, 51.93°N and 4.79°E). Also this station is located in an energy-limited region where 94% of the days show no water limitation and where the impact of groundwater on evaporation is small.

5.1.1.3. Groundwater Level

The groundwater level dynamics over The Netherlands are represented well by GLEAM-Hydro with a median correlation of $R_{\text{median}} = 0.78$ (Table 1). The median correlation is only slightly better with LHM, despite the latter being calibrated for The Netherlands (Table 1 and Figure 2d). In both models, correlations are greater than 0.5 at 88% of the sites, with a standard deviation (σ) in the correlations of $R_\sigma = 0.21$. LHM shows slightly better median RMSE and KGE values than GLEAM-Hydro (Table 1). Based on the correlation coefficients, 44% of the sites perform better or similarly well with GLEAM-Hydro compared to LHM (62% based on RMSE, 34% based on KGE). Figure 3a shows an example of a station where GWL are estimated better with GLEAM-Hydro than LHM (GLEAM-Hydro: $R = 0.64$, RMSE = 0.05 m, KGE = 0.62, LHM: $R = 0.22$, RMSE = 1.37 m, KGE = -1.36), whereas Figure 3b illustrates the opposite (GLEAM-Hydro: $R = 0.85$, RMSE = 0.67 m, KGE = 0.45, LHM: $R = 0.92$, RMSE = 0.12 m, KGE = 0.80).

At multiple sites, significant biases are detected in the simulated groundwater level (see Figure A2 in the Appendix). The groundwater level bias in GLEAM-Hydro is a result of the bias in the initial conditions. In GLEAM-Hydro (LHM), RMSE is smaller than 5 m at 97% (96%) of the sites.

Overall, the groundwater representation in GLEAM-Hydro is able to mimic the skill of LHM in simulating GWL. The degree of uncertainty, that is, the variation in the performance metrics, in GLEAM-Hydro is comparable to LHM (Figure 2d).

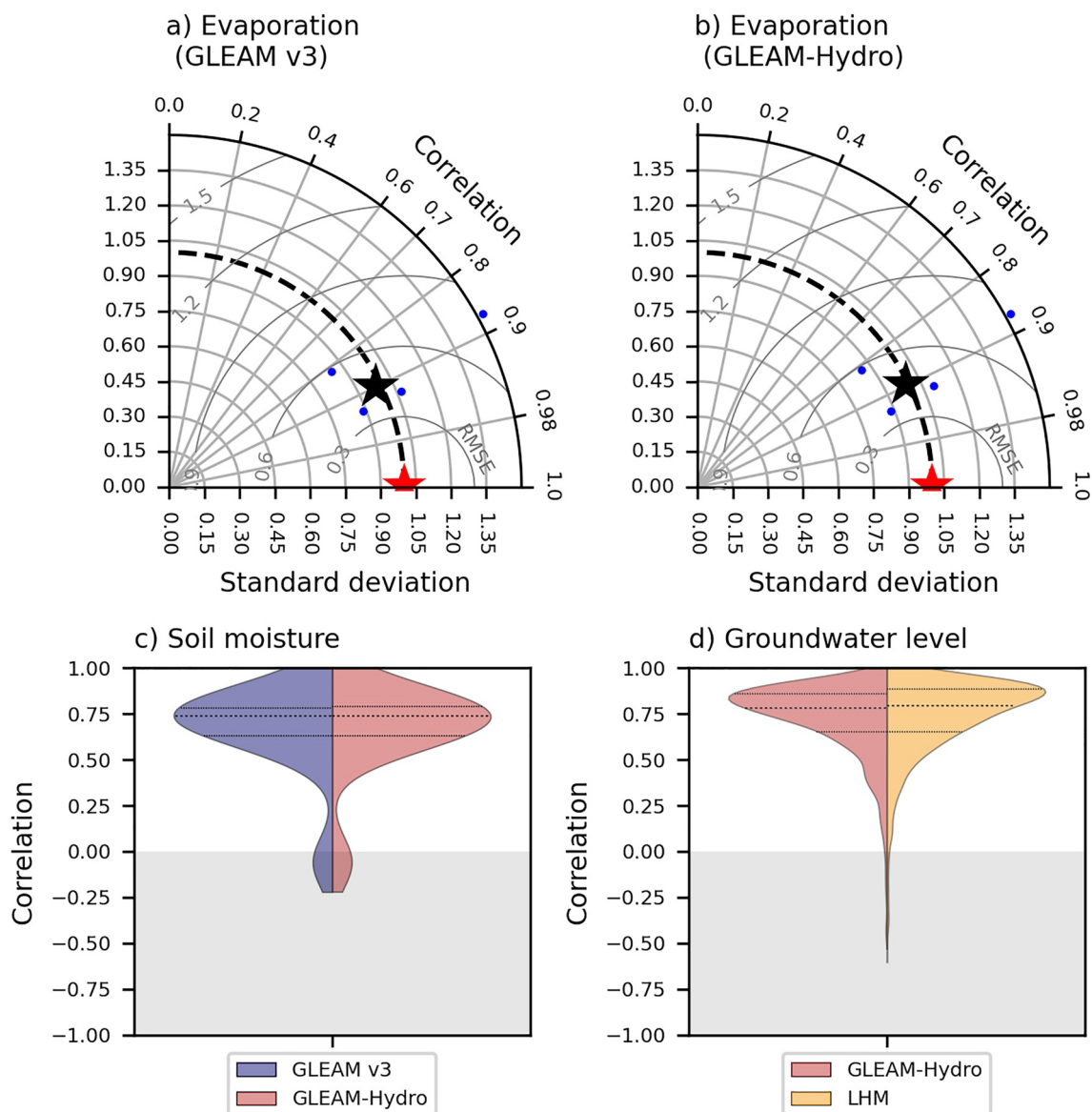


Figure 2. (a)–(b) Taylor diagrams illustrating the performance of (a) Global Land Evaporation Amsterdam Model (GLEAM) v3 and (b) GLEAM-Hydro with respect to evaporation for The Netherlands. The standard deviation and root mean square error are normalized using the standard deviation of the observed time series such that the red star serves as the reference point. (c)–(d) Violin plots illustrating the validation of (c) soil moisture and (d) groundwater level based on the correlation.

5.1.2. Global Validation

5.1.2.1. Evaporation

Across all eddy-covariance stations available globally, evaporation from GLEAM v3 is already represented well with a median correlation of $R_{\text{median}} = 0.81$, which is similar to previous studies (Martens et al., 2017). The remaining performance metrics amount to $RMSE_{\text{median}} = 1.01 \text{ mm day}^{-1}$ and $KGE_{\text{median}} = 0.49$ for GLEAM v3 (Table 2). Incorporating groundwater in GLEAM-Hydro does not influence the median performances significantly (see Figure 4 and Table 2) as, again, many stations are located in regions with energy-limited conditions or deep GWL (see Figure A1a in the Appendix). Note that in only 39% of the continental surface, long-term mean GWL simulated by GLEAM-Hydro are shallower than -2.5 m . When considering only stations where groundwater becomes a relevant water source for transpiration (8 out of 100 stations), then the median correlation improves from $R_{\text{GLEAMv3}} = 0.66$ to $R_{\text{GLEAM-Hydro}} = 0.69$ (Figure 4c and Table 2), indicating the temporal dynamics of evaporation are better simulated if groundwater is considered as a source for transpiration. In this

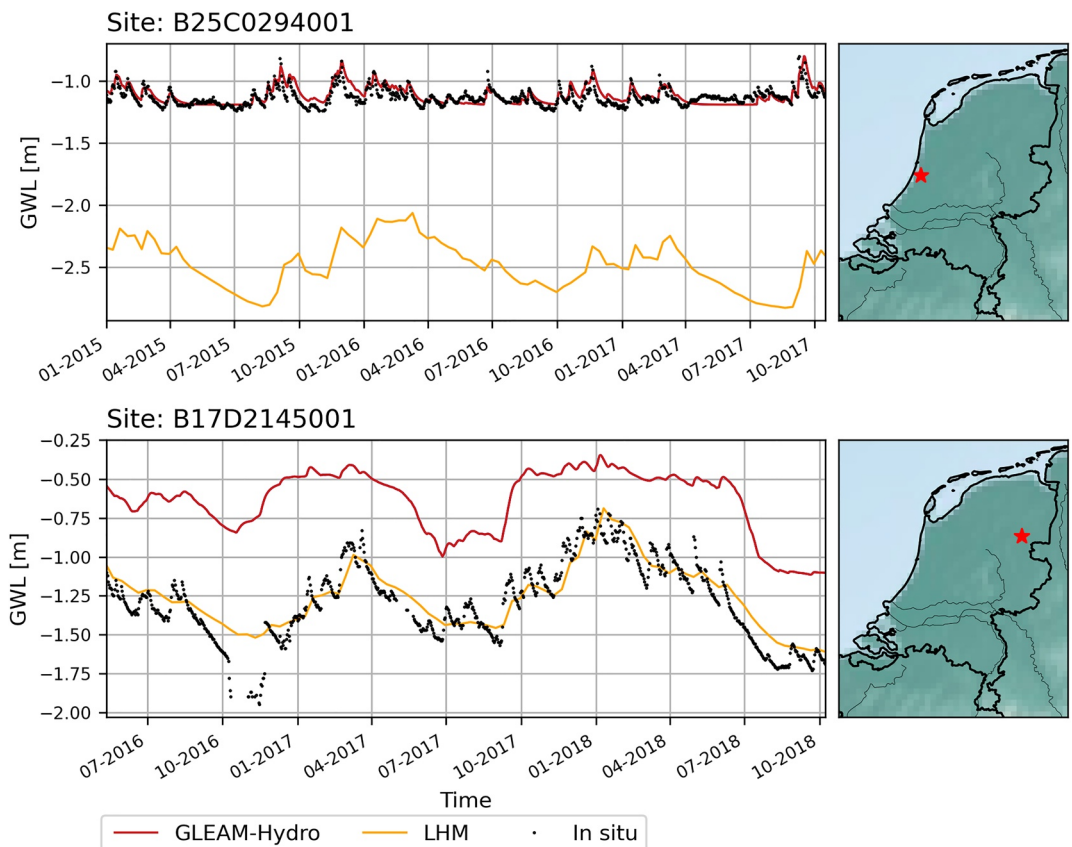


Figure 3. Time series of groundwater levels at two sample locations in The Netherlands, comparing GLEAM-Hydro and Landelijk Hydrologisch Model (LHM) with observations from corresponding well observations. The sites are located in (a) the province North-Holland (52.33°N and 4.64°E), and (b) the province Drenthe (52.72°N and 6.53°E).

study, groundwater is considered a relevant water source for transpiration in regions where evaporation increases by more than 1 mm day^{-1} on at least 1 day within the record, which reflects stations with groundwater access and high potential evaporation relative to the soil water availability, that is, water limited conditions. The improvement is not reflected in the median *KGE* and *RMSE* values (see Table 2), as only four of the eight stations improved with respect to *RMSE* and *KGE*. See Figure 5 for an example eddy-covariance station in Italy, where the incorporation of groundwater in the model influences evaporation and increases the accuracy of the estimates. There, the maximum evaporation increase due to groundwater access is 2.5 mm day^{-1} . The correlation increases from $R = 0.82$ in GLEAM v3 to $R = 0.89$ in GLEAM-Hydro, and the *RMSE* and *KGE* change from $\text{RMSE} = 0.82 \text{ mm day}^{-1}$ and $\text{KGE} = 0.82$ (GLEAM v3) to $\text{RMSE} = 0.89 \text{ mm day}^{-1}$ and $\text{KGE} = 0.68$ (GLEAM-Hydro).

5.1.2.2. Soil Moisture

The soil moisture from GLEAM v3 is represented well at most sites with $R_{\text{median}} = 0.71$ (Table 2), which is similar to previous studies (Beck et al., 2021; Martens et al., 2017). The remaining performance metrics amount to $\text{RMSE}_{\text{median}} = 9.49\%$ and $\text{KGE}_{\text{median}} = 0.26$. Similar to evaporation, the soil moisture performance does not change substantially when incorporating plant access to groundwater (see Figure 4d and Table 2). The differences remain small also when validating only for sites where groundwater becomes a relevant water source for transpiration (Table 2), which is the case for 143 out of 3,422 sites (see Figure A1b in the Appendix). At those sites,

Table 2

Median Statistics for Different Variables and Global Land Evaporation Amsterdam Model Versions With Respect to All Stations Globally, and in Brackets With Respect to Stations Where Groundwater Is a Relevant Water Source

Median values	GLEAM v3	GLEAM-Hydro	Unit
Evaporation	R	0.81 (0.66)	0.81 (0.69)
	RMSE	1.01 (1.20)	mm day^{-1}
	KGE	0.49 (0.32)	—
Soil moisture	R	0.71 (0.67)	0.71 (0.63)
	RMSE	9.49 (9.44)	%
	KGE	0.26 (0.30)	—
Groundwater	R	n/a	0.22 (-0.03)
	RMSE	n/a	m
	KGE	n/a	-0.87 (-0.86)

Note. Performance metrics include correlation (*R*), root mean square error (*RMSE*), and Kling-Gupta Efficiency (*KGE*).

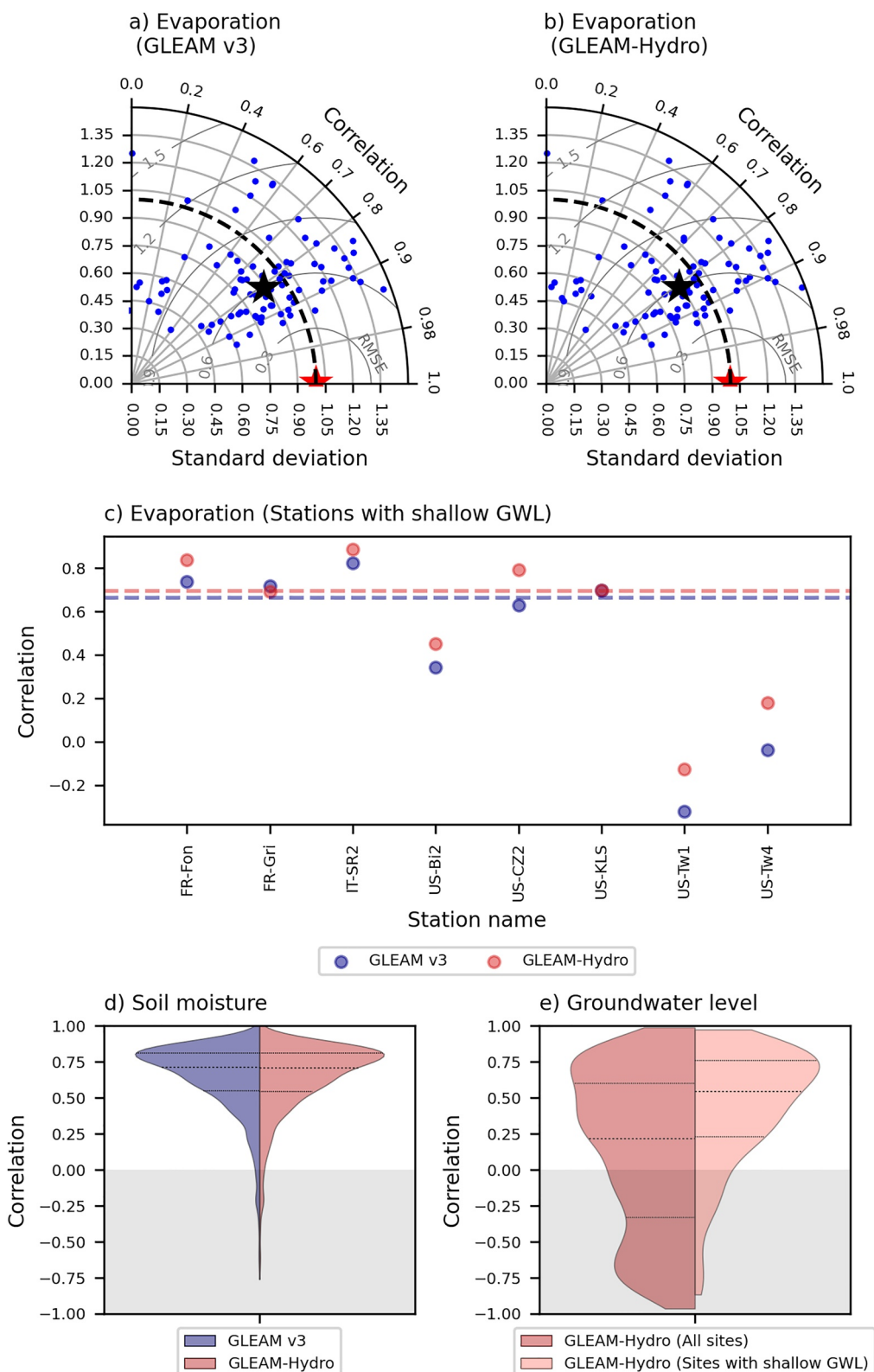


Figure 4.

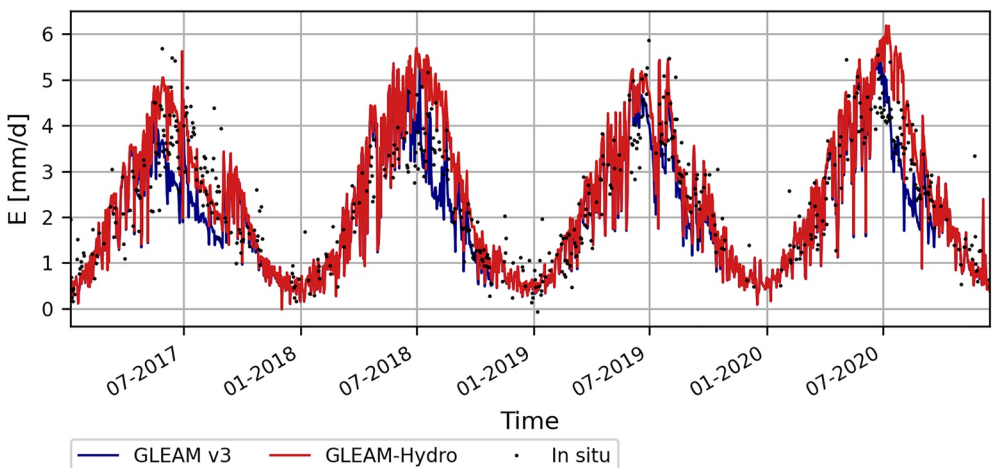


Figure 5. Evaporation at the eddy-covariance tower San Rossore 2 in Italy (IT-SR2 at 43.73°N and 10.29°E) and as simulated with Global Land Evaporation Amsterdam Model (GLEAM v3) and GLEAM-Hydro.

the performance metrics change slightly, without clear signals for improvement, from $R = 0.67$, $RMSE = 9.44\%$ and $KGE = 0.30$ for GLEAM v3 to $R = 0.63$, $RMSE = 9.13\%$ and $KGE = 0.26$ for GLEAM-Hydro (Table 2). Note, that changes in the soil moisture only occur indirectly through altered transpiration (see Section 2.1.4): If plants have access to groundwater, they extract less water from the unsaturated zone. Thus, in GLEAM-Hydro, soil moisture is generally higher than in GLEAM v3 if plants have access to groundwater (see Figure A3).

5.1.2.3. Runoff

Over all stations, the long-term mean runoff over the simulation period is represented reasonably well with GLEAM v3 compared to the discharge observations, with $R = 0.84$ (Figure A4a in the Appendix). The median MD is equal to $MD_{\text{median}} = -123.2 \text{ mm year}^{-1}$ (Figure A4b in the Appendix), largely reflecting biases in precipitation and/or the simulated evaporation. The median percent bias amounts to $PBIAS_{\text{median}} = 40.4\%$. Overall, runoff is overestimated at 11 of the 97 stations with GLEAM v3, and underestimated at 81 stations. Runoff is simulated well at five stations, where only small biases (i.e., $|MD| < 10 \text{ mm year}^{-1}$) are found.

Incorporating plant access to groundwater in GLEAM-Hydro leads to a slight correlation increase ($R = 0.85$), and the MD changes between $\Delta MD = 0.0\text{--}30.7 \text{ mm year}^{-1}$ with $\Delta MD = MD_{\text{GLEAM v3}} - MD_{\text{GLEAM-Hydro}}$. Changes in the percent bias range between $\Delta PBIAS = -105.6\%$ to 40.6% ($\Delta PBIAS = PBIAS_{\text{GLEAM v3}} - PBIAS_{\text{GLEAM-Hydro}}$) with positive values indicating runoff improved with GLEAM-Hydro (Figures A4c and A4d in the Appendix). At 61 of the 97 stations, runoff changes are small ($|\Delta PBIAS| < 1\%$) as groundwater access is limited in the basins associated with these stations.

Compared to GLEAM v3, evaporation in GLEAM-Hydro either increases when groundwater is a relevant source for transpiration or remains the same when the groundwater level is too deep. Hence, based on Equation 11 the long-term mean runoff can only decrease or remain the same. Therefore, the skill of those stations that overestimate runoff with GLEAM v3 (11 of 97 stations) improve (8 stations) or remain the same (3 stations). On the other hand, at those stations that already underestimate runoff with GLEAM v3 (81 of 97 stations), the bias further increases with GLEAM-Hydro, except when the roots have no access to the groundwater level. This results in a decreased accuracy at 24 of the 81 stations that already underestimate runoff with GLEAM v3.

5.1.2.4. Groundwater Level

The global groundwater level performance varies considerably among the 1,329 sites (Figure 4e). The median correlation of simulated GWL in GLEAM-Hydro with observations is equal to $R_{\text{median}} = 0.22$. This increases

Figure 4. (a)–(b) Taylor diagrams illustrating the global performance of (a) Global Land Evaporation Amsterdam Model (GLEAM) v3 and (b) GLEAM-Hydro with respect to evaporation. The standard deviation and root mean square error are normalized using the standard deviation of the observed time series such that the red star serves as the reference point. (c) Correlation of evaporation simulated with GLEAM v3 (blue) and GLEAM-Hydro (red) against observations at those eddy-covariance stations that are influenced by groundwater. The dashed line indicates the median correlation over the selected stations. (d)–(e) Violin plots illustrating the validation of (d) soil moisture and (e) groundwater level based on the correlation.

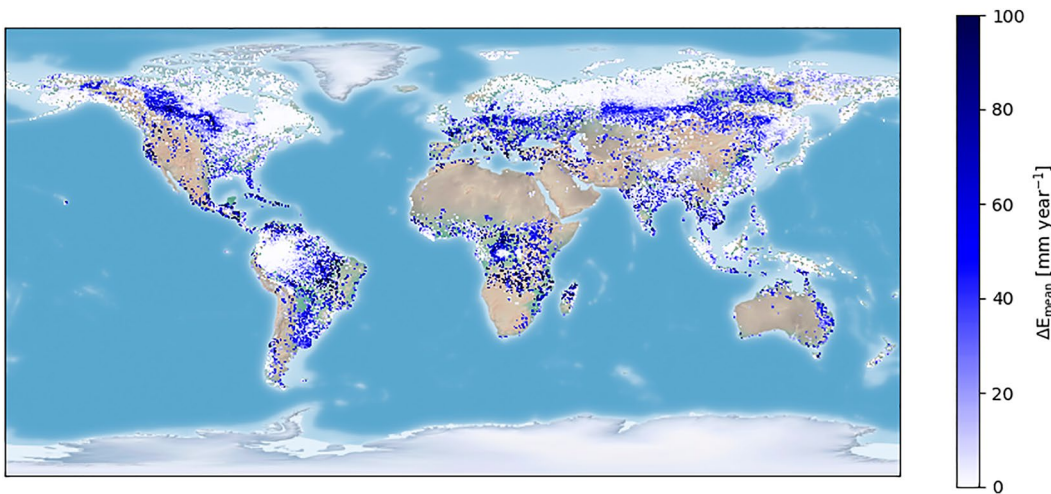


Figure 6. Average evaporation increase due to the incorporation of plant access to groundwater in Global Land Evaporation Amsterdam Model (GLEAM) ($\Delta E = E_{\text{GLEAM-Hydro}} - E_{\text{GLEAM v3}}$) averaged over the study period. Regions with $\Delta E < 0.01 \text{ mm year}^{-1}$ are masked out.

to $R_{\text{median}} = 0.54$ when considering only those sites with shallow water table depths, that is, where plants have access to the groundwater system based on the modeled or observed GWL. The remaining performance metrics amount to $RMSE_{\text{median}} = 1.60 \text{ m}$ and $KGE_{\text{median}} = -0.87$ when considering all sites (Table 2). The correlation is greater than 0.5 at 31% of the sites (Figure A5 in the Appendix) and $RMSE$ is smaller than 5 m at 62% of the sites (Figure A6 in the Appendix). As an example, Figure A7 in the Appendix shows the time series of observed and simulated groundwater level for a well-represented station near Philadelphia in the United States (at 74.84°W and 39.99°N , $R = 0.85$, $RMSE = 0.21 \text{ m}$, $KGE = 0.83$).

5.2. Global Influence of Groundwater on Evaporation

Representing plant access to groundwater increases the annual-mean, globally-averaged terrestrial evaporation from 392.4 to $394.8 \text{ mm year}^{-1}$. This corresponds to an increase of 2.5 mm year^{-1} globally-averaged; the standard deviation of all land pixels amounts to $11.0 \text{ mm year}^{-1}$. In other words, the terrestrial evaporation increases by $404 \text{ km}^3 \text{ year}^{-1}$ over the continental surface, from $74,064 \text{ km}^3 \text{ year}^{-1}$ (GLEAM v3) to $74,468 \text{ km}^3 \text{ year}^{-1}$ (GLEAM-Hydro). Relative to GLEAM v3, the annual-mean, globally-averaged evaporation increases by 0.5% with a standard deviation of 2.2%. The globally-averaged groundwater contribution to evaporation f_{GW} is 0.008 with a standard deviation of 0.03, that is, around 0.8% of the global evaporation is sourced from groundwater.

The maximum local increase of annual-mean evaporation is $245.2 \text{ mm year}^{-1}$ (Figure 6) or 149.7% relative to GLEAM v3 (Figure A8 in the Appendix). The local annual groundwater contribution to evaporation f_{GW} reaches values up to 0.36, thus groundwater can supply more than one-third of the annual evaporation at specific locations. At the daily scale, evaporation increases locally up to 5.5 mm day^{-1} . Large evaporation increases are observed in, for example, Canada, Russia, and several regions in Congo and South America. In those regions, the groundwater level is shallow (Fan et al., 2013) as illustrated in Figure A9 in the Appendix. Hence, groundwater-sourced evaporation is, as expected, strongly influenced by the groundwater level (Figures 7a–7f).

Groundwater-sourced evaporation is highest in drylands, that is, in regions with an aridity index larger than 1.5 (Figure 7). In addition, it is higher for tall vegetation compared to short vegetation and bare soil (Figure 7)—which is expected given the deeper roots of tall vegetation (see Section 2.1.1). The annual-mean groundwater-sourced evaporation in drylands, where plants have groundwater access, is 468.2 and $138.1 \text{ mm year}^{-1}$ for tall and short vegetation, respectively. This corresponds to a mean groundwater contribution to transpiration of $f_{\text{GW}} = 0.67$ and $f_{\text{GW}} = 0.24$ for tall and short vegetation, respectively. This discrepancy between the groundwater contributions to transpiration is causing much lower groundwater contributions averaged over all land cover types of an entire grid-cell (Figure A10). At the grid-cell level, the annual-mean groundwater-sourced evaporation is lower in drylands ($25.6 \text{ mm year}^{-1}$) than in non-drylands ($31.6 \text{ mm year}^{-1}$) when considering only regions with

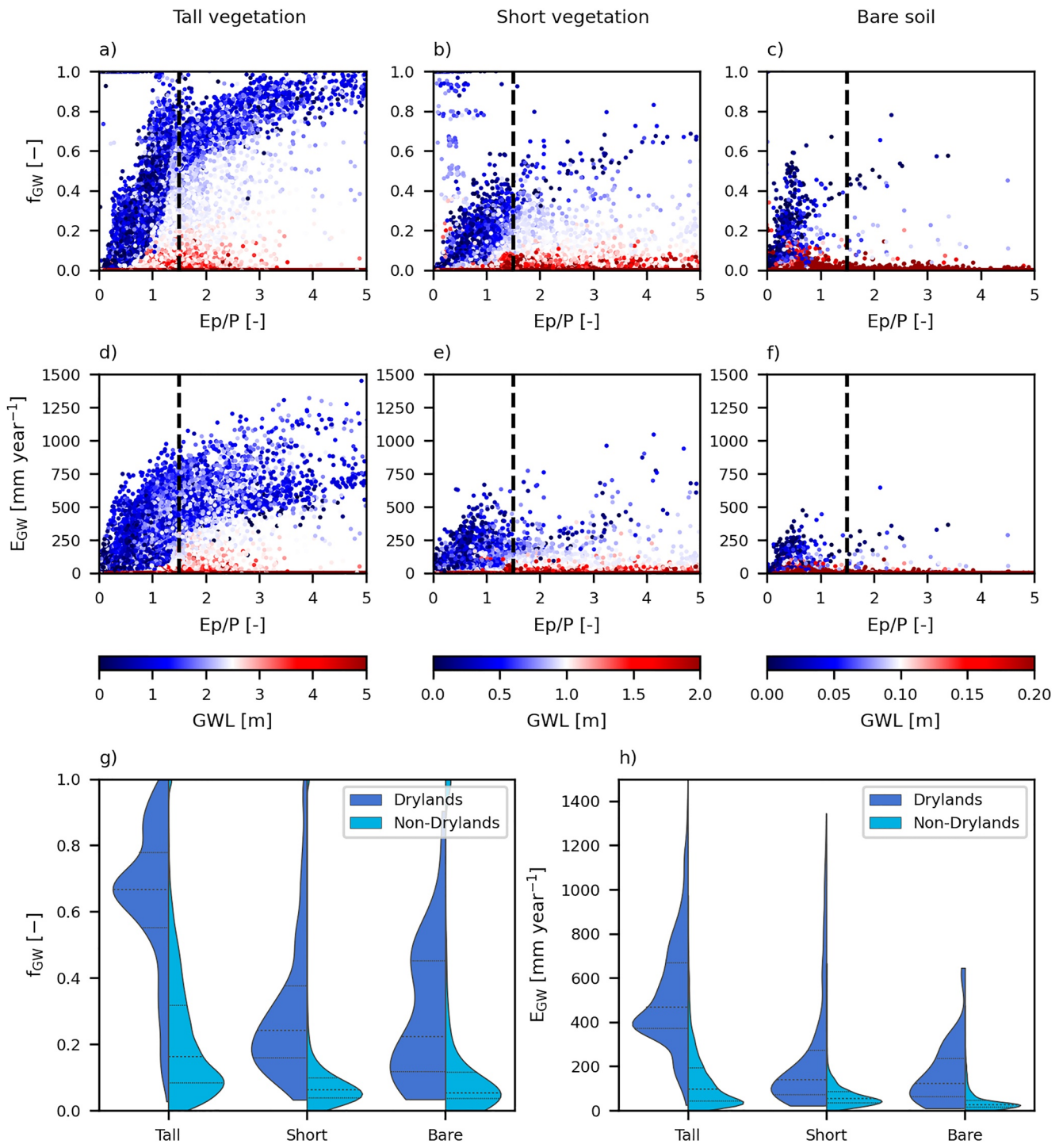


Figure 7. Groundwater contribution fraction (f_{GW}) and groundwater-sourced evaporation (E_{GW}) for tall vegetation, short vegetation and bare soil (a)–(f) as a function of aridity (E_p/P) and groundwater levels (GWL), and (g)–(h) distinguishing between drylands ($E_p/P > 1.5$) and non-drylands ($E_p/P < 1.5$). Subplots (g)–(h) consider only regions with groundwater access. All results are averaged over the study period.

groundwater access, that is, $E_{GW,annual-mean} > 0$. Relatively speaking, the groundwater contribution is lower in drylands ($f_{GW} = 0.03$) than in non-drylands ($f_{GW} = 0.04$), resulting from the fact that less tall and short vegetation exist in drylands (Figures A10d–A10f).

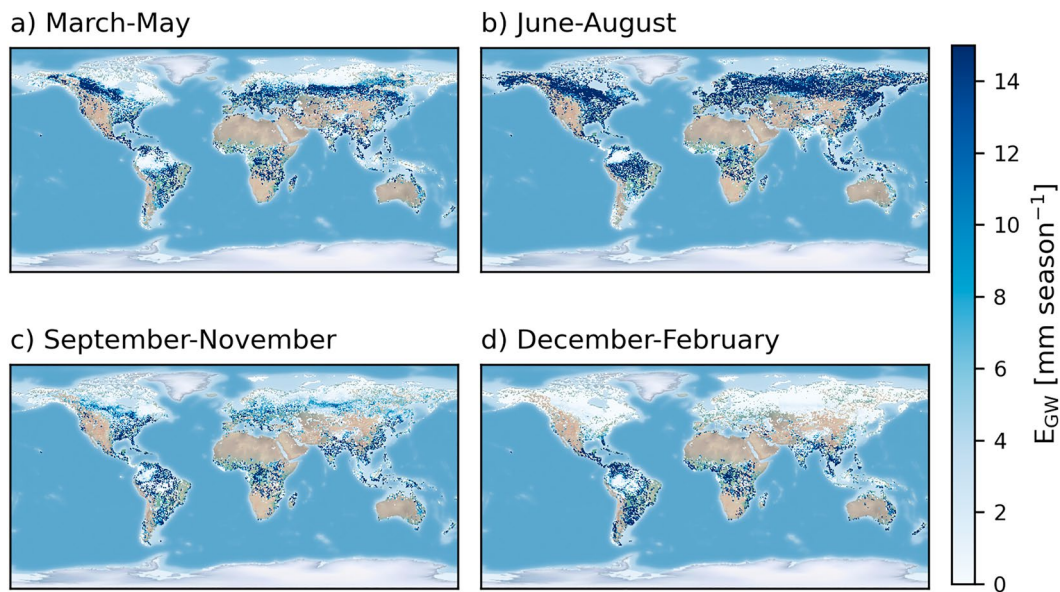


Figure 8. Seasonal groundwater-sourced evaporation. Regions with no groundwater access at any time within the record are masked out.

The groundwater contribution to evaporation varies seasonally with higher values in the Northern Hemisphere (NH, $f_{GW} = 0.01\text{--}0.04$) than in the Southern Hemisphere (SH, $f_{GW} = 0.007\text{--}0.02$) when excluding regions without groundwater access at any time within the record (Figures A11a and A11b). However, groundwater-sourced evaporation shows more extreme seasonal variations in the NH ($E_{GW} = 0.05\text{--}11.2 \text{ mm season}^{-1}$) compared to the SH ($E_{GW} = 2.1\text{--}4.8 \text{ mm season}^{-1}$)—see Figures 8, A11c, and A11d. In the NH, the groundwater-sourced evaporation is most pronounced in summer (June–August). Annual fluctuations are limited to $f_{GW} = 0.02\text{--}0.03$ (NH) and $f_{GW} = 0.003\text{--}0.01$ (SH), excluding the year 2015 where higher values are likely still affected by the initial condition (Figure A11). The annual variation in E_{GW} is limited to $10.9\text{--}19.2 \text{ mm year}^{-1}$ (NH) and $2.4\text{--}13.7 \text{ mm year}^{-1}$ (SH); with the lowest values in 2021 for both hemispheres.

6. Discussion

This study enables a better understanding of evaporation during water-stressed conditions by introducing groundwater-sourced evaporation in a satellite-based model. The simulated groundwater contribution to transpiration in GLEAM-Hydro is based on knowledge gained from previous studies (Balugani et al., 2017; Barbetta & Peñuelas, 2017; Maxwell & Condon, 2016; Miguez-Macho & Fan, 2021; Tfwala et al., 2021); see Section 1. Incorporating groundwater interactions increases the annual-mean, globally-averaged evaporation by 2.5 mm year^{-1} and locally by up to $245.2 \text{ mm year}^{-1}$. The globally-averaged contribution of groundwater to evaporation in GLEAM-Hydro ($f_{GW} = 0.008$) is similar to findings by Miguez-Macho and Fan (2021) of approximately 1%. Also, Barbetta and Peñuelas (2017) show a median $f_{GW} = 0.56$ for tall vegetation in dry seasons which is similar to the findings of this study ($f_{GW} = 0.67$, Figure 7g). The spatial pattern of the groundwater contribution in this study differs considerably from previous studies (e.g., Miguez-Macho & Fan, 2021) and shows higher contributions in, for example, Canada, Russia and Congo where the GWL are shallow (Figure A9 in the Appendix). These differences may be attributed to uncertainties in the evaporation estimates in both this study (as discussed below) and previous studies.

6.1. Sources of Uncertainties

There are several sources of uncertainty in the proposed approach to incorporate plant access to groundwater. First, this approach assumes lateral groundwater flow is insignificant at the chosen spatial resolution, which is plausible based on findings in previous studies (Krakauer et al., 2014). Second, this approach does not include capillary rise nor the existence of roots deeper than 2.5 m tapping into the groundwater system. Furthermore, we

assume that there is no direct interaction between groundwater and the unsaturated zone (see also Section 2.1.4). These interactions are only mimicked through plants extracting (part of the) water from the groundwater, provided they have access to it, resulting in less extraction from the unsaturated zone and hence increased soil moisture (Figure A3). That is also why the simulated soil moisture changes only marginally and the skill of soil moisture does not improve from GLEAM v3 to GLEAM-Hydro at the limited observation sites available (see Section 5.1.2). Moreover, results are sensitive to data uncertainties, including initial GWL and soil properties. Last but not least, results here are constrained to the processes represented in GLEAM, which does not explicitly model, among others, human impacts such as pumping and irrigation, preferential flow, the impact of vapor pressure deficit (VPD) on evaporation, and processes related to (weathered) bedrock water, which has been proven to be an important water source for transpiration (Jiménez-Rodríguez et al., 2022; McCormick et al., 2021; Rempe & Dietrich, 2018). These are all potential avenues for improvements in the future, but are considered outside the scope of this study.

To reduce uncertainties related to the groundwater representation of GLEAM-Hydro, GLEAM could be coupled to a groundwater model (e.g., MODFLOW). Its impact on evaporation is illustrated for The Netherlands by using LHM-based GWL as forcing in GLEAM (i.e., GLEAM-LHM). Compared to GLEAM-Hydro, GLEAM-LHM reproduces the spatial pattern of evaporation (Figure A12 in the Appendix). However, the annual-mean evaporation for the region increases even more with GLEAM-LHM (4.8 mm year^{-1} or 0.2% relative to GLEAM v3) than with GLEAM-Hydro (2.4 mm year^{-1} or 0.1%). It is noted, however, that two-way coupling between evaporation and groundwater was not considered in GLEAM-LHM.

Furthermore, the coarse resolution of 0.25° applied in this study introduces uncertainties due to sub-grid topographical heterogeneity. This impacts water table depth estimates and hence whether or not plants have access to groundwater. This source of uncertainty is not unique to this model but is valid for many global models run at coarse resolutions (Bierkens, 2015; Lawrence et al., 2019; Lovato et al., 2022; Müller Schmied et al., 2021; Yoshida et al., 2022). To analyze the effect of this uncertainty on evaporation, GLEAM-Hydro is run at 1 km resolution for The Netherlands using LHM-based GWL as initial conditions, instead of using the global map by Fan et al. (2017). Differences between GLEAM-Hydro and GLEAM v3 are evaluated at both 1 and 25 km resolution. This experiment shows that the annual-mean evaporation increase through groundwater access is lower in the 1 km version (2.9 mm year^{-1}) than in the 25 km version ($13.1 \text{ mm year}^{-1}$). Local differences are most pronounced during water-limited conditions as illustrated in Figure A13 for the drought of 2018. In many regions, plants have more frequent access to groundwater at the coarse resolution resulting in higher total evaporation. At Cabauw, the higher evaporation in the 25 km version corresponds better with the field observations (Figure A13c). Only increasing the spatial resolution has a larger effect on the annual-mean evaporation ($82.9 \text{ mm year}^{-1}$ decrease for GLEAM v3) than incorporating groundwater, but this is more likely a result of different input data (such as soil properties) and missing processes at the high resolution (such as lateral groundwater flow). This agrees with Reinecke et al. (2020) who show that the skill of groundwater level simulations does not improve substantially when increasing the spatial resolution alone.

Validation results presented here are sensitive to spatial heterogeneity within a grid cell such that an observation site may not be representative of an entire grid scale. Nevertheless, this approach allows us to evaluate the change in performance from the benchmark GLEAM v3 to the new GLEAM-Hydro, since these representativeness errors are (in principle) not systematic from site to site.

6.2. Future Studies

Future studies should address the limitations mentioned above. For instance, we recommend improving the definition of the maximum root depth by using global datasets, instead of constant values per vegetative fraction worldwide. In addition, estimated groundwater level dynamics could be improved further by using total water storage anomalies as observed from satellites (Landerer & Swenson, 2012; Swenson & Wahr, 2006) for data assimilation. The proposed approach for groundwater–vegetation interactions could further be tested at higher resolutions. However, note that this may require additional modifications since currently missing processes such as lateral groundwater flow may become significant at finer scales (de Graaf & Stahl, 2022; Reinecke et al., 2020). Furthermore, it would be very valuable if new eddy-covariance stations, located in dry regions and combined with groundwater level and root depth field observations, are available. This would benefit the verification of groundwater access and validation of evaporation at

locations where groundwater becomes relevant. Unfortunately, most eddy-covariance stations used here are located in regions with deep water tables (according to Fan et al. (2013)) or in energy-limited regions with abundant water. As such, the effect of groundwater on evaporation could only be validated at a limited number of in situ stations. The consideration of additional forcing variables such as VPD in GLEAM has recently been explored using a hybrid approach (Koppa et al., 2022). Recent improvements in specific modules, such as the inclusion of groundwater-sourced evaporation presented here, will be brought together in the next GLEAM version (v4).

7. Conclusion

The goal of this study was to enable a better understanding of evaporation during water-stressed conditions by incorporating plant access to groundwater in existing large-scale evaporation estimates, and to assess the impact of groundwater on evaporation globally. To that end, a novel, conceptual approach to estimate groundwater–vegetation interactions was developed. It connected conceptual elements of groundwater reservoirs and (observed) groundwater contributions to transpiration. This approach was incorporated into GLEAM, yielding the GLEAM-Hydro version of the model.

The impact of groundwater on evaporation was analyzed globally by comparing GLEAM v3 with GLEAM-Hydro: While the globally-averaged annual-mean evaporation increased only by 2.5 mm year⁻¹ (0.5%), local changes in regions with a shallow water table were much higher (up to 245.2 mm year⁻¹). The groundwater contribution to transpiration was highest for tall vegetation under dry conditions ($f_{GW} = 0.63$) due to more frequent plant access to groundwater. In general, little improvements were found in the simulation of evaporation as the majority of the eddy-covariance stations was located in regions with no groundwater access or energy-limited regions, where the impact of groundwater on evaporation was marginal. However, at 75% of the stations where groundwater was a relevant water source, the temporal dynamics of the simulated evaporation improved. The skill of the model, also for other variables such as soil moisture and discharge, remained more or less unaltered. The skill of GLEAM-Hydro to simulate GWL was further demonstrated through the comparison to a dedicated regional groundwater model (LHM). For The Netherlands, where abundant water table observations were available, both models showed considerable skill. However, LHM performed better in terms of RMSE and KGE which was to be expected for a groundwater model calibrated for The Netherlands.

The presented approach paves the way toward the integration of groundwater in, for example, land surface and hydrological models and other algorithms that aim to derive evaporation from, for example, satellite-based observations. Representing groundwater in GLEAM also sets the ground to assimilate satellite gravimetry data in the future (Giroto et al., 2017). This approach is a first step toward more realistic evaporation estimates during water-stressed conditions in global, satellite-based models.

Appendix A

Additional figures and tables are provided in this appendix. They give an overview of the field observations used (Figure A1 and Table A2) and visualize the performance of GLEAM-Hydro with respect to soil moisture, groundwater level and runoff (Figures A2–A7 and Table A2). In addition, they illustrate the impact of groundwater on evaporation (Figures A8–A13).

Table A1
In Situ Observations Used in This Study

Source	Long name	Data type	Nr stations	Website, citation	Coverage
AmeriFlux	—	Radiation, meteorological & soil moisture data	512	https://ameriflux.lbl.gov/ (AmeriFlux, 2021)	Global
DINO	<i>Data en Informatie van de Nederlandse Ondergrond</i>	Groundwater level data	2,750	https://www.dinoloket.nl/standen (Data en Informatie van de Nederlandse Ondergrond (DINO), 2021)	The Netherlands
EFDC	European Fluxes Database Cluster	Radiation, meteorological & soil moisture data	88	http://www.europe-fluxdata.eu/ (European Fluxes Database Cluster (EFDC), 2021)	Global
FLUXNET-CH4	—	Radiation, meteorological & soil moisture data	67	https://fluxnet.org/ , (Delwiche et al., 2021; Knox et al., 2019; Pastorello et al., 2020)	Global
GRDC	Global Runoff Data Center	Discharge data	108	https://www.bafg.de/GRDC/EN/Home/homepage_node.html (Global Runoff Data Center (GRDC), 2021)	Global
ICOS	Integrated Carbon Observation System	Radiation, meteorological & soil moisture data	145	https://www.icos-cp.eu/ (ICOS RI, 2021)	Global
IGRAC	International Groundwater Resources Assessment Center	Groundwater level data	5,359	https://ggis.un-igrac.org/view/ggmn (International Groundwater Resources Assessment Center (IGRAC), 2021)	Global
ISMN	International Soil Moisture Network	Meteorological & soil moisture data	4,672	https://ismn.geo.tuwien.ac.at/en/ , (W. A. Dorigo et al., 2011; W. Dorigo et al., 2013, 2021)	Global

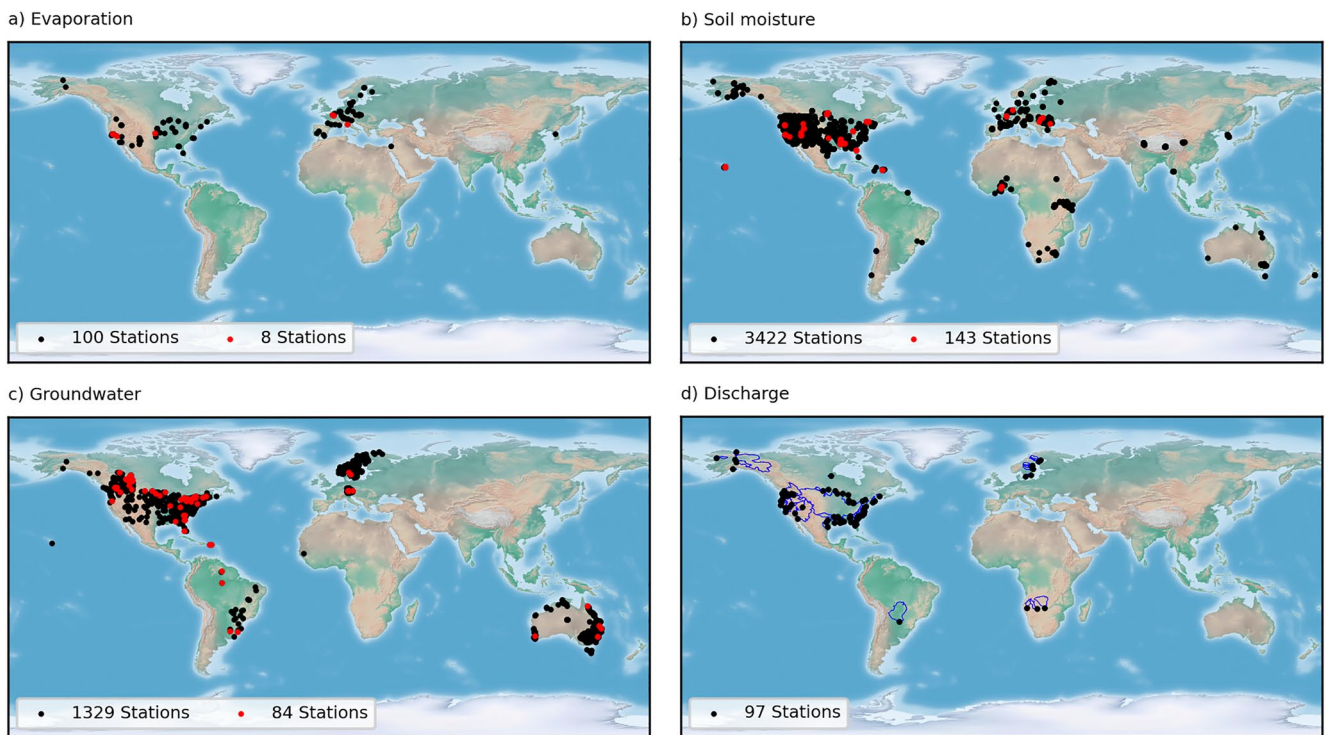


Figure A1. Map of stations with (a) evaporation, (b) soil moisture, (c) groundwater level, and (d) discharge stations (including basin outline in blue) used in this study. Black dots indicate all stations used, and red dots indicate stations where groundwater becomes a relevant source for evaporation.

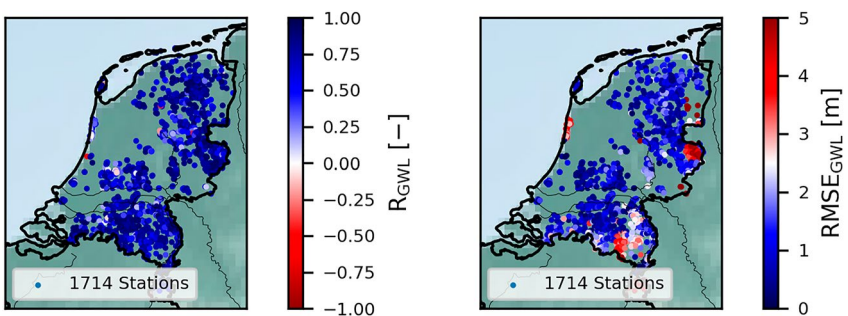


Figure A2. Groundwater level validation results in The Netherlands: (a) correlation and (b) RMSE.

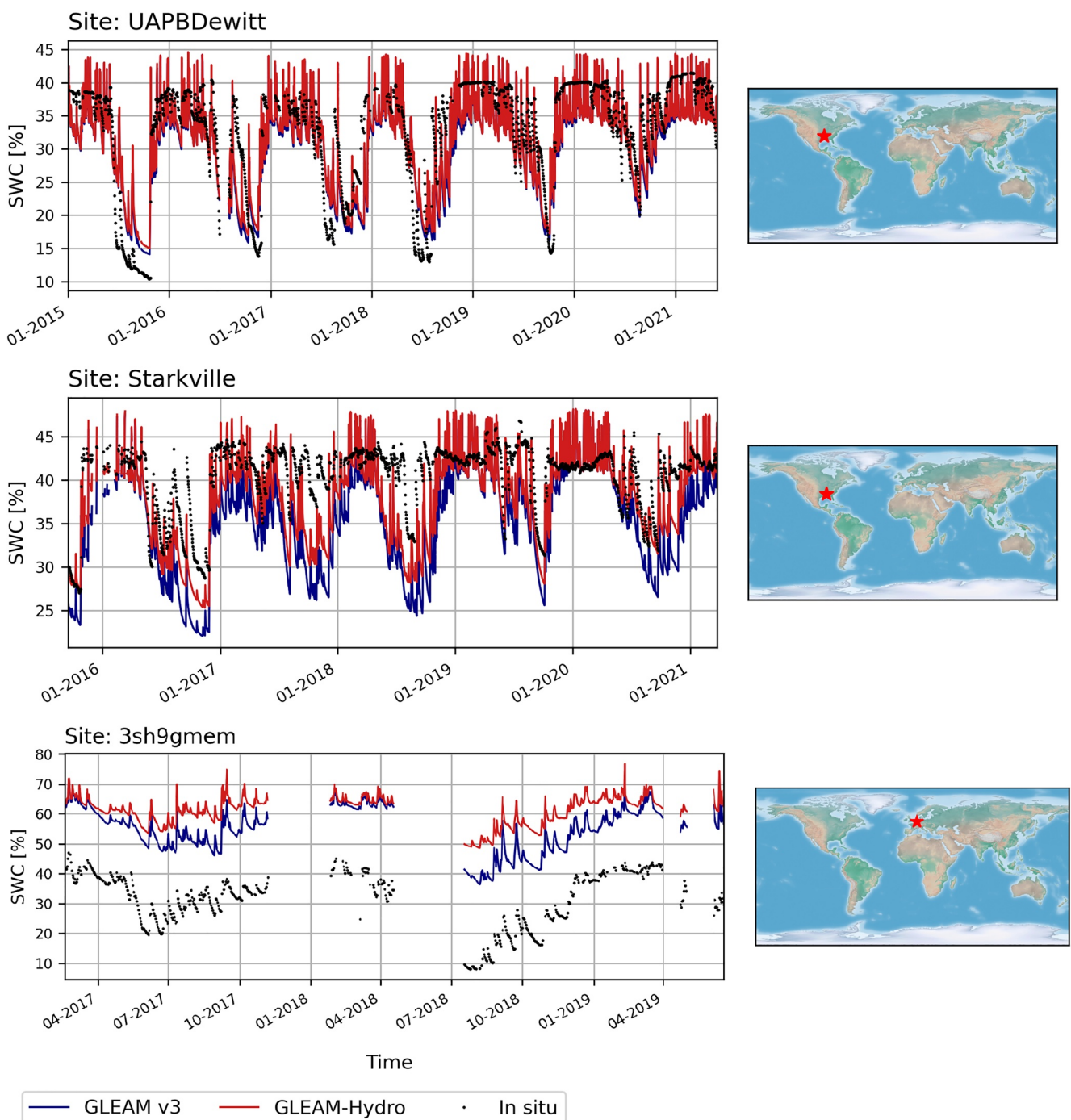


Figure A3. Soil moisture time-series according to field observations, Global Land Evaporation Amsterdam Model (GLEAM) v3 and GLEAM-Hydro at three locations. See Table A2 for their coordinates and correlation values.

Table A2

Soil Moisture Correlation With Respect to Three International Soil Moisture Network Field Observations for Global Land Evaporation Amsterdam Model v3 and GLEAM-Hydro

Site	Latitude	Longitude	Depth (m)	GLEAM v3	GLEAM-Hydro
Starkville	33.63	-88.77	0.20	0.64	0.65
UAPBDeWitt	34.28	-91.35	0.10	0.82	0.82
3sh9gmem	51.93	4.79	0.05	0.88	0.84

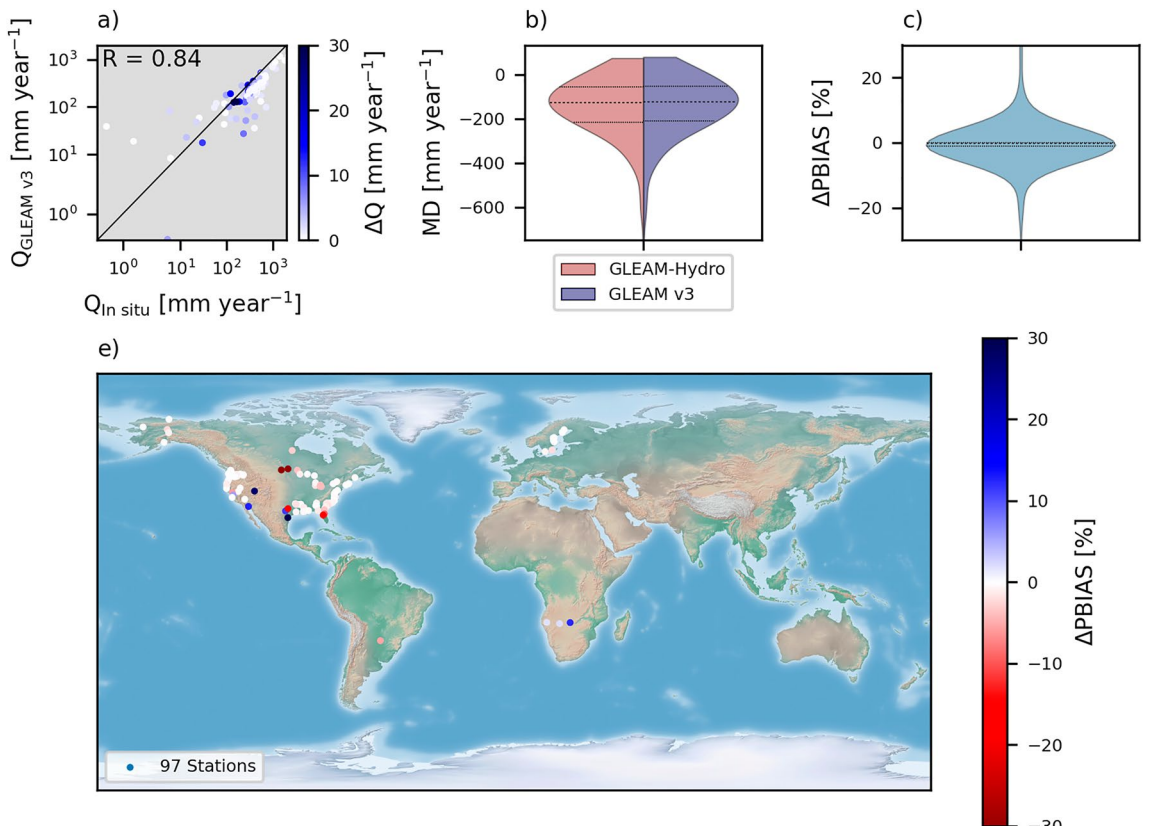


Figure A4. Runoff performance. (a) Long-term average runoff according to in situ data (x-axis) versus Global Land Evaporation Amsterdam Model (GLEAM) v3 (y-axis) and with $\Delta Q_{\text{GLEAM}} = Q_{\text{GLEAMv3}} - Q_{\text{GLEAM-Hydro}}$ for the colors. (b) Mean difference (MD) for GLEAM v3 and GLEAM-Hydro with positive values indicating the GLEAM-based runoff are overestimated. (c) Difference in PBIAS (i.e., $\Delta \text{PBIAS} = \text{PBIAS}_{\text{GLEAMv3}} - \text{PBIAS}_{\text{GLEAM-Hydro}}$). (d) Spatial pattern of ΔPBIAS with positive values indicating the bias improves in GLEAM-Hydro.

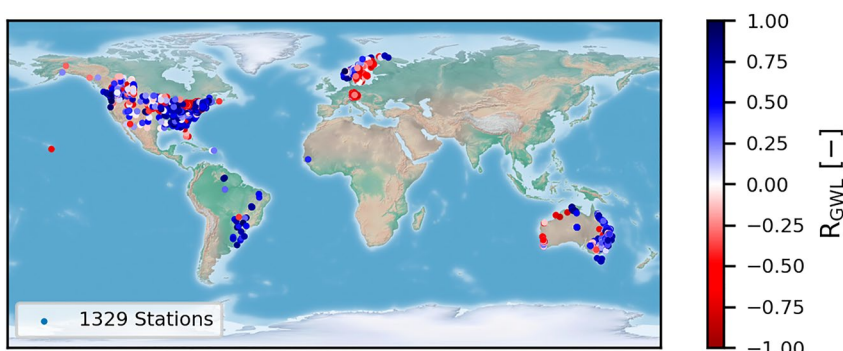


Figure A5. Global groundwater level validation results: Correlation.

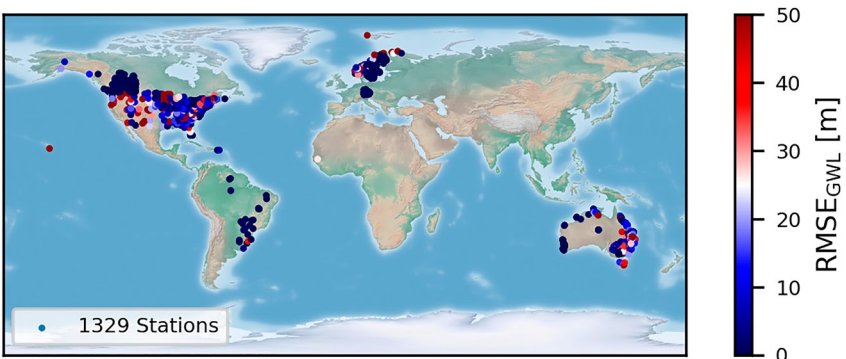


Figure A6. Global groundwater level validation results: *RMSE*.

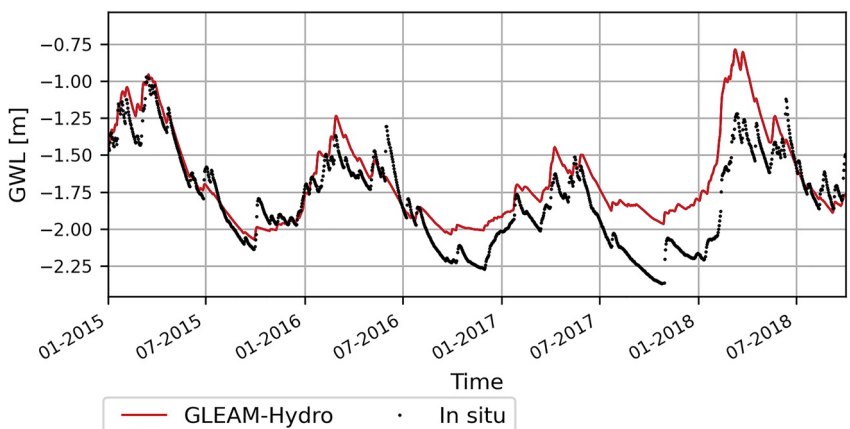


Figure A7. Groundwater levels at a well represented station near Philadelphia in the United States (74.84°W and 39.99°N).

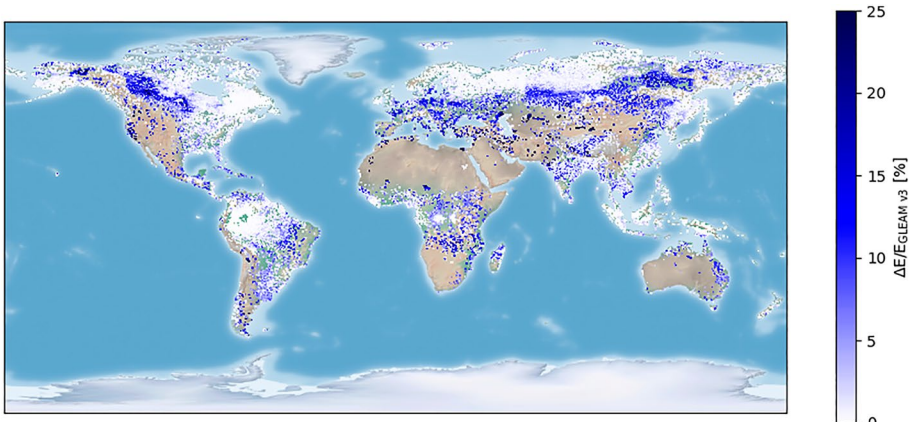


Figure A8. Average evaporation increase due to the incorporation of plant access to groundwater in Global Land Evaporation Amsterdam Model (GLEAM) ($\Delta E = E_{\text{GLEAM-Hydro}} - E_{\text{GLEAMv3}}$) relative to GLEAM v3 averaged over the study period. Regions with $\frac{\Delta E}{E_{\text{GLEAMv3}}} < 0.01\%$ are masked out.

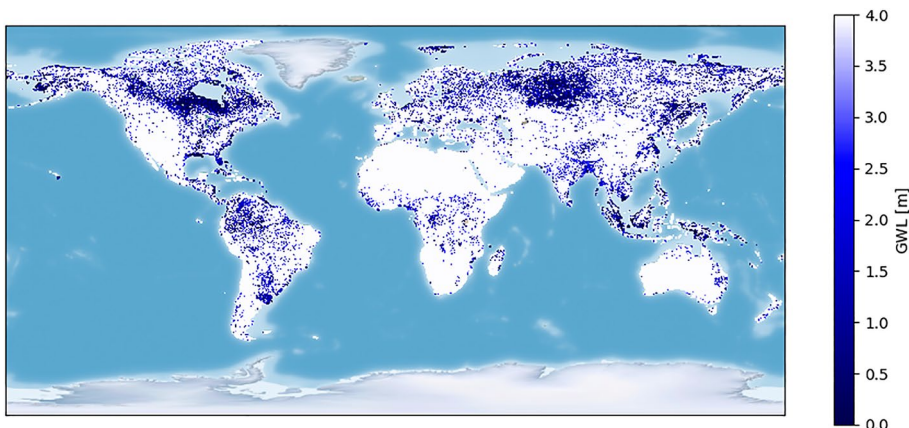


Figure A9. Initial groundwater level based on (Fan et al., 2013).

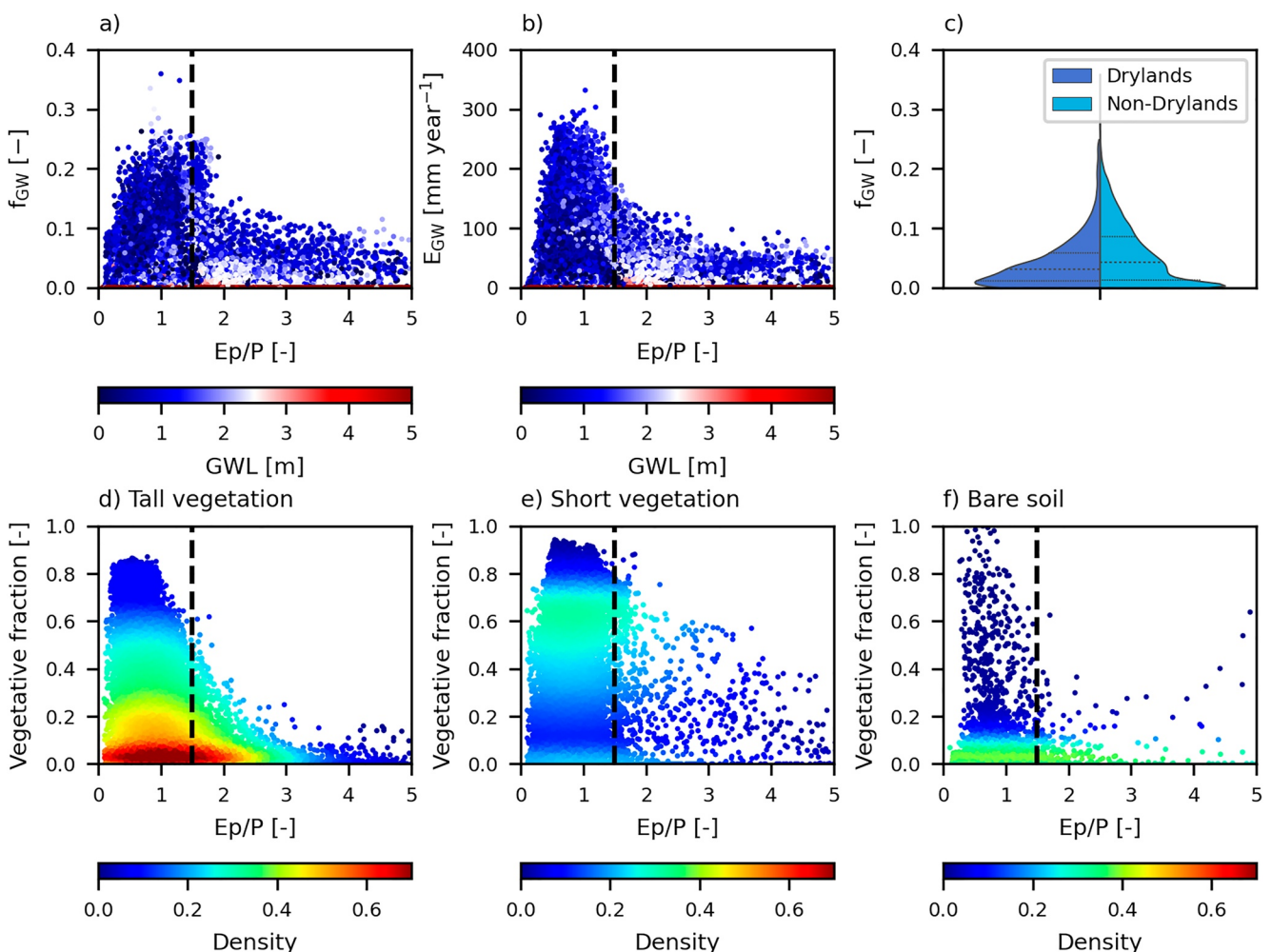


Figure A10. (a) Groundwater contribution fraction (f_{GW}) and (b) groundwater-sourced evaporation (E_{GW}) aggregated over entire grid-cells as a function of aridity (E_p/P) and groundwater levels (GWL). (c) Violin plot of f_{GW} distinguishing between drylands ($E_p/P > 1.5$) and non-drylands ($E_p/P < 1.5$). Vegetative fraction for (d) tall vegetation, (e) short vegetation and (f) bare soil as a function of the aridity with the colors indicating the density of the dots. Subplots (c)–(f) consider only regions with groundwater access. All results are averaged over the study period.

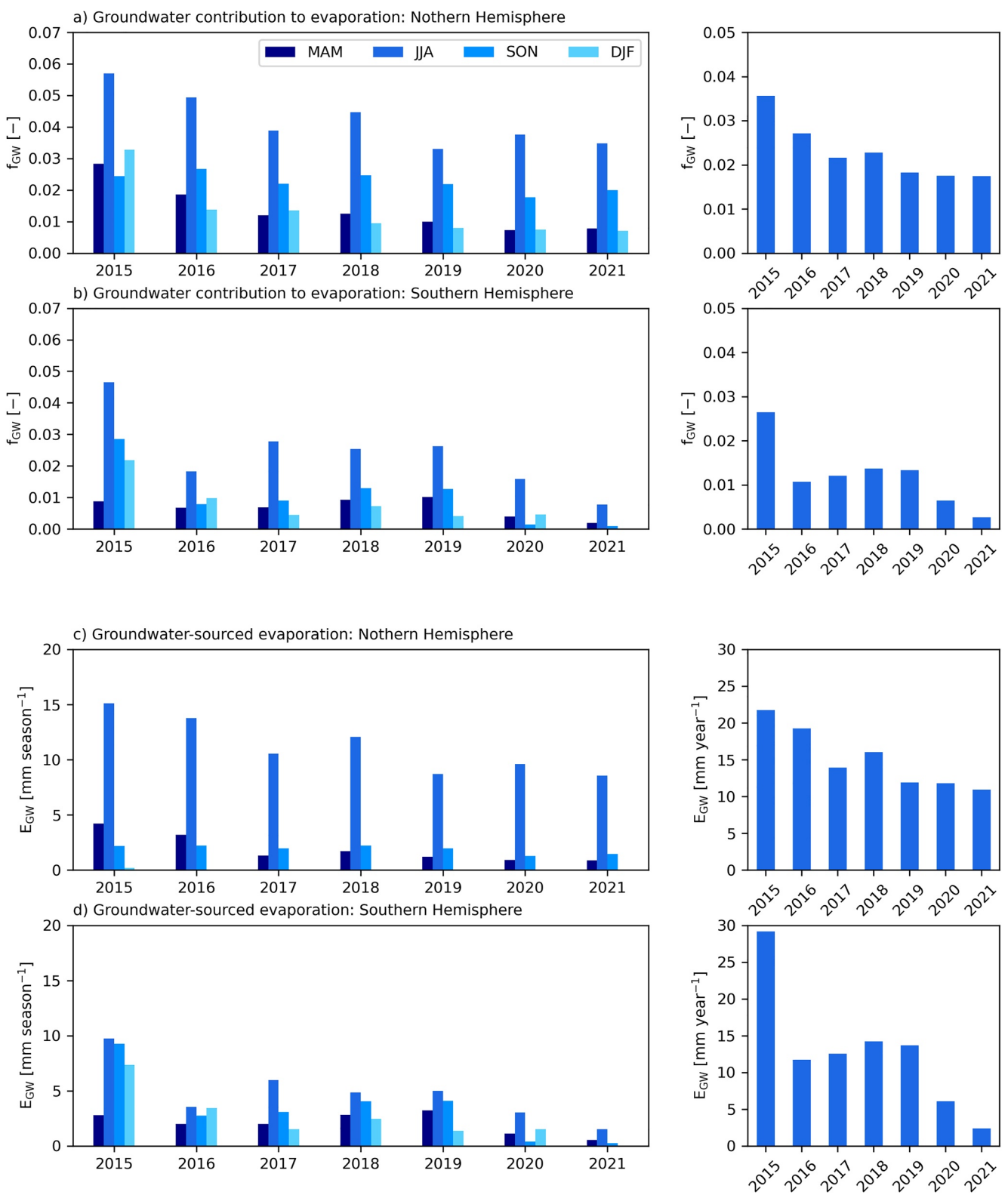


Figure A11. Seasonal and annual variation in the (a)–(b) groundwater contribution to evaporation (f_{GW}) and (c)–(d) groundwater-sourced evaporation (E_{GW}) for the Northern (a and c) and Southern (b and d) Hemisphere.

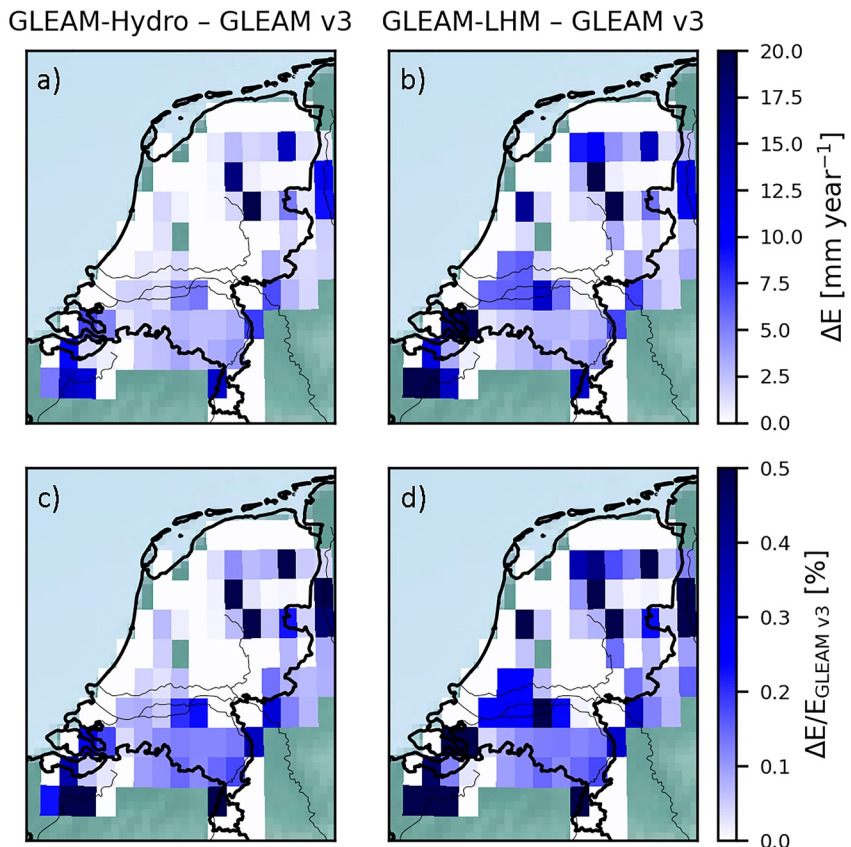


Figure A12. Average evaporation increase in The Netherlands due to the incorporation of plant access to groundwater in Global Land Evaporation Amsterdam Model (GLEAM). Subplots (a)–(b) illustrate absolute differences, subplots (c)–(d) relative differences. Subplots (a) and (c) use GLEAM-Hydro, subplots (b) and (d) use GLEAM-LHM. Absolute difference: $\Delta E = E_{\text{GLEAM-Hydro/LHM}} - E_{\text{GLEAMv3}}$, relative difference: $\frac{\Delta E}{E_{\text{GLEAMv3}}}$.

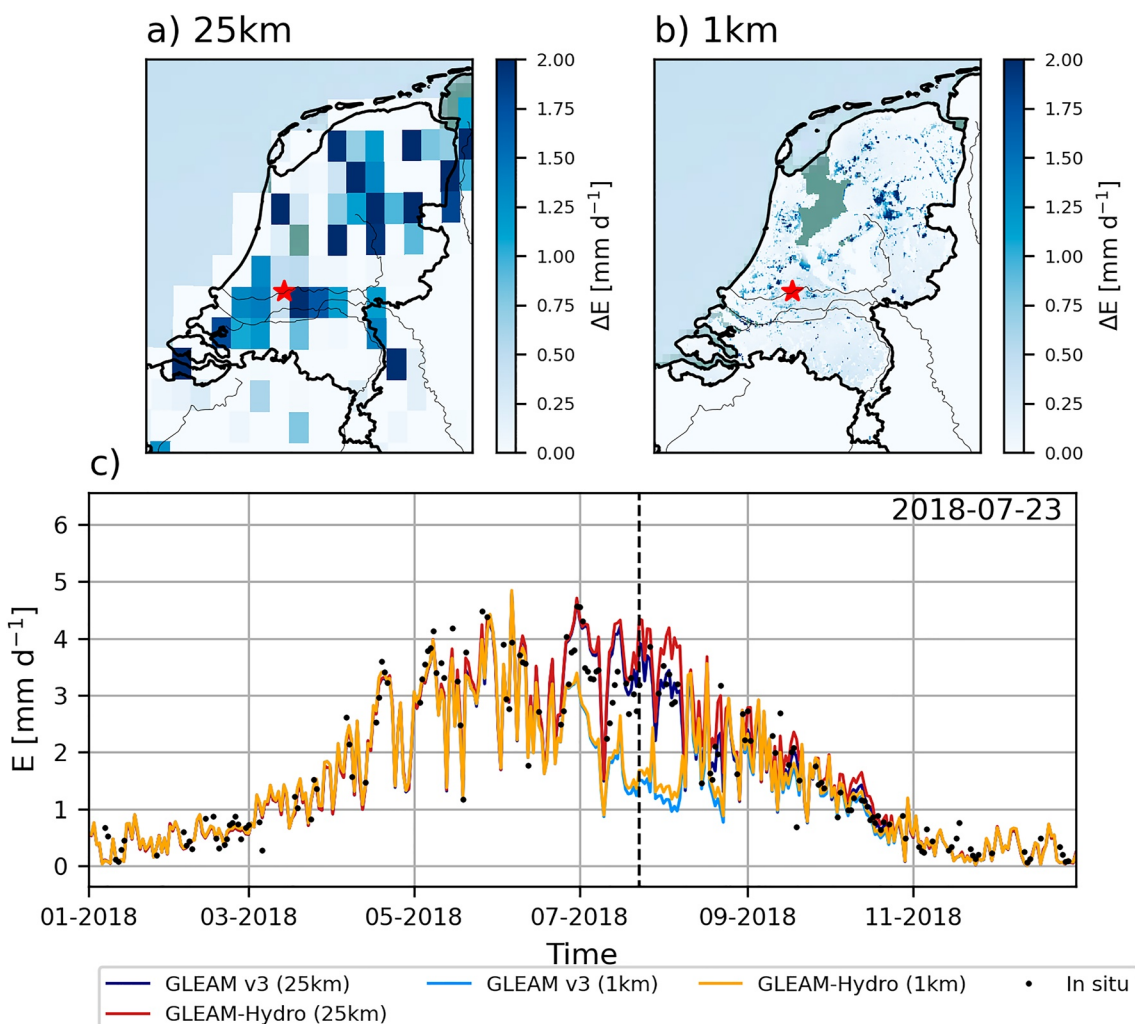


Figure A13. Evaporation increase of GLEAM-Hydro relative to Global Land Evaporation Amsterdam Model (GLEAM) v3 at (a) 25 km and (b) 1 km resolution on 23 July 2018. (c) Evaporation time-series at Cabauw (51.93°N and 4.79°E) according to GLEAM v3 and GLEAM-Hydro at 25 and 1 km resolution for the year 2018.

Data Availability Statement

All in situ observations were downloaded in June/July 2021 from multiple platforms as shown in Table A1. The authors are thankful to all PIs who have shared their data through the platforms AmeriFLUX, DINO, EFDC, FLUXNET, GRDC, ICOS, IGRAC, and ISMN. GLEAM output data that are generated in this study and are required to reproduce the main results and figures, are available at <https://doi.org/10.5281/zenodo.7099512>.

Acknowledgments

This study was funded by the European Space Agency (ESA) through the projects DTE Hydrology Evolution (Contract no. ESA 4000136272/21/I-EF—CCN N. 1) and 4DMED-Hydrology (Contract no. ESA 4000136272/21/I-EF). AK and DM acknowledge support from the European Union Horizon 2020 Programme (DOWN2EARTH, 869550) and the European Research Council (HEAT, 101088405).

References

- Amanambu, A. C., Obarein, O. A., Mossa, J., Li, L., Ayeni, S. S., Balogun, O., et al. (2020). Groundwater system and climate change: Present status and future considerations. *Journal of Hydrology*, 589, 125163. <https://doi.org/10.1016/j.jhydrol.2020.125163>
- AmeriFlux. (2021). Lawrence Berkeley National Laboratory. Retrieved from <https://ameriflux.lbl.gov/>
- Aumann, H., Chahine, M., Gautier, C., Goldberg, M., Kalnay, E., McMillin, L., et al. (2003). AIRS/AMSU/HSB on the aqua mission: Design, science objectives, data products, and processing systems. *IEEE Transactions on Geoscience and Remote Sensing*, 41(2), 253–264. <https://doi.org/10.1109/TGRS.2002.808356>
- Balugani, E., Lubczynski, M., Reyes-Acosta, L., van der Tol, C., Francés, A., & Metselaar, K. (2017). Groundwater and unsaturated zone evaporation and transpiration in a semi-arid open woodland. *Journal of Hydrology*, 547, 54–66. <https://doi.org/10.1016/j.jhydrol.2017.01.042>
- Barbeta, A., & Peñuelas, J. (2017). Relative contribution of groundwater to plant transpiration estimated with stable isotopes. *Scientific Reports*, 7(1), 10580. <https://doi.org/10.1038/s41598-017-09643-x>
- Bastiaanssen, W., Menenti, M., Feddes, R., & Holtslag, A. (1998). A remote sensing surface energy balance algorithm for land (SEBAL). 1. Formulation. *Journal of Hydrology*, 212–213, 198–212. [https://doi.org/10.1016/S0022-1694\(98\)00253-4](https://doi.org/10.1016/S0022-1694(98)00253-4)

- Beck, H. E., Pan, M., Miralles, D. G., Reichle, R. H., Dorigo, W. A., Hahn, S., et al. (2021). Evaluation of 18 satellite- and model-based soil moisture products using in situ measurements from 826 sensors. *Hydrology and Earth System Sciences*, 25(1), 17–40. <https://doi.org/10.5194/hess-25-17-2021>
- Beck, H. E., Wood, E. F., Pan, M., Fisher, C. K., Miralles, D., van Dijk, A. I., et al. (2019). MSWEP v2 global 3-hourly 0.1° precipitation: Methodology and quantitative assessment. *Bulletin of the American Meteorological Society*, 100(3), 473–502. <https://doi.org/10.1175/BAMS-D-17-0138.1>
- Beyer, M., Hamutoko, J., Wanke, H., Gaj, M., & Koeniger, P. (2018). Examination of deep root water uptake using anomalies of soil water stable isotopes, depth-controlled isotopic labeling and mixing models. *Journal of Hydrology*, 566, 122–136. <https://doi.org/10.1016/j.jhydrol.2018.08.060>
- Bieger, K., Arnold, J. G., Rathjens, H., White, M. J., Bosch, D. D., Allen, P. M., et al. (2017). Introduction to SWAT+, a completely restructured version of the soil and water assessment tool. *JAWRA Journal of the American Water Resources Association*, 53(1), 115–130. <https://doi.org/10.1111/1752-1688.12482>
- Bierkens, M. F. P. (2015). Global hydrology 2015: State, trends, and directions. *Water Resources Research*, 51(7), 4923–4947. <https://doi.org/10.1002/2015WR017173>
- Blyth, E. M., Arora, V. K., Clark, D. B., Dadson, S. J., De Kauwe, M. G., Lawrence, D. M., et al. (2021). Advances in land surface modelling. *Current Climate Change Reports*, 7(2), 45–71. <https://doi.org/10.1007/s40641-021-00171-5>
- Clark, M. P., Fan, Y., Lawrence, D. M., Adam, J. C., Bolster, D., Gochis, D. J., et al. (2015). Improving the representation of hydrologic processes in earth system models. *Water Resources Research*, 51(8), 5929–5956. <https://doi.org/10.1002/2015WR017096>
- Condon, L. E., Kollet, S., Bierkens, M. F. P., Fogg, G. E., Maxwell, R. M., Hill, M. C., et al. (2021). Global groundwater modeling and monitoring: Opportunities and challenges. *Water Resources Research*, 57(12), e2020WR029500. <https://doi.org/10.1029/2020WR029500>
- Data en Informatie van de Nederlandse Ondergrond (DINO). (2021). TNO innovation for life. Retrieved from <https://www.dinoloket.nl/standen>
- de Graaf, I. E. M., & Stahl, K. (2022). A model comparison assessing the importance of lateral groundwater flows at the global scale. *Environmental Research Letters*, 17(4), 044020. <https://doi.org/10.1088/1748-9326/ac50d2>
- de Graaf, I. E. M., van Beek, R. L., Gleeson, T., Moosdorf, N., Schmitz, O., Sutanudjaja, E. H., & Bierkens, M. F. (2017). A global-scale two-layer transient groundwater model: Development and application to groundwater depletion. *Advances in Water Resources*, 102, 53–67. <https://doi.org/10.1016/j.advwatres.2017.01.011>
- De Lange, W. J., Prinsen, G. F., Hoogewoud, J. C., Veldhuizen, A. A., Verkaik, J., Oude Essink, G. H., et al. (2014). An operational, multi-scale, multi-model system for consensus-based, integrated water management and policy analysis: The Netherlands hydrological instrument. *Environmental Modelling & Software*, 59, 98–108. <https://doi.org/10.1016/j.envsoft.2014.05.009>
- Delwiche, K. B., Knox, S. H., Malhotra, A., Fluet-Chouinard, E., McNicol, G., Feron, S., et al. (2021). FLUXNET-CH₄: A global, multi-ecosystem dataset and analysis of methane seasonality from freshwater wetlands. *Earth System Science Data*, 13(7), 3607–3689. <https://doi.org/10.5194/essd-13-3607-2021>
- DiMiceli, C., Carroll, M., Sohlberg, R., Kim, D., Kelly, M., & Townshend, J. (2015). MOD44B MODIS/Terra vegetation continuous fields yearly L3 global 250m SIN grid V006 [Dataset]. NASA EOSDIS Land Processes DAAC. <https://doi.org/10.5067/MODIS/MOD44B.006>
- Dorigo, W., Himmelbauer, I., Aberer, D., Schremmer, L., Petrakovic, I., Zappa, L., et al. (2021). The International Soil Moisture Network: Serving earth system science for over a decade. *Hydrology and Earth System Sciences*, 25(11), 5749–5804. <https://doi.org/10.5194/hess-25-5749-2021>
- Dorigo, W., Xaver, A., Vreugdenhil, M., Gruber, A., Hegyiiová, A., Sanchis-Dufau, A., et al. (2013). Global automated quality control of in situ soil moisture data from the international soil moisture network. *Vadose Zone Journal*, 12(3), vzej2012.0097. <https://doi.org/10.2136/vzej2012.0097>
- Dorigo, W. A., Wagner, W., Hohensinn, R., Hahn, S., Paulik, C., Xaver, A., et al. (2011). The international soil moisture network: A data hosting facility for global in situ soil moisture measurements. *Hydrology and Earth System Sciences*, 15(5), 1675–1698. <https://doi.org/10.5194/hess-15-1675-2011>
- European Fluxes Database Cluster (EFDC). (2021). Retrieved from <http://www.europe-fluxdata.eu/>
- Evaristo, J., & McDonnell, J. J. (2017). Prevalence and magnitude of groundwater use by vegetation: A global stable isotope meta-analysis. *Scientific Reports*, 7(1), 44110. <https://doi.org/10.1038/srep44110>
- Fan, Y. (2015). Groundwater in the Earth's critical zone: Relevance to large-scale patterns and processes. *Water Resources Research*, 51(5), 3052–3069. <https://doi.org/10.1002/2015WR017037>
- Fan, Y., Li, H., & Miguez-Macho, G. (2013). Global patterns of groundwater table depth. *Science*, 339(6122), 940–943. <https://doi.org/10.1126/science.1229881>
- Fan, Y., Miguez-Macho, G., Jobbágé, E., Jackson, R., & Otero-Casal, C. (2017). Hydrologic regulation of plant rooting depth. *Proceedings of the National Academy of Sciences*, 114(40), 10572–10577. <https://doi.org/10.1073/pnas.1712381114>
- Fenicia, F., Savenije, H. H. G., Matgen, P., & Pfister, L. (2006). Is the groundwater reservoir linear? Learning from data in hydrological modelling. *Hydrology and Earth System Sciences*, 10(1), 139–150. <https://doi.org/10.5194/hess-10-139-2006>
- Fisher, J. B., Melton, F., Middleton, E., Hain, C., Anderson, M., Allen, R., et al. (2017). The future of evapotranspiration: Global requirements for ecosystem functioning, carbon and climate feedbacks, agricultural management, and water resources. *Water Resources Research*, 53(4), 2618–2626. <https://doi.org/10.1002/2016WR020175>
- Fisher, J. B., Tu, K. P., & Baldocchi, D. D. (2008). Global estimates of the land–atmosphere water flux based on monthly AVHRR and ISLSCP-II data, validated at 16 FLUXNET sites. *Remote Sensing of Environment*, 112(3), 901–919. <https://doi.org/10.1016/j.rse.2007.06.025>
- Frappart, F., Wigneron, J.-P., Li, X., Liu, X., Al-Yaari, A., Fan, L., et al. (2020). Global monitoring of the vegetation dynamics from the vegetation optical depth (VOD): A review. *Remote Sensing*, 12(18), 2915. <https://doi.org/10.3390/rs12182915>
- Gao, H., Hrachowitz, M., Fenicia, F., Gharari, S., & Savenije, H. H. G. (2014). Testing the realism of a topography-driven model (FLEX-Topo) in the nested catchments of the Upper Heihe, China. *Hydrology and Earth System Sciences*, 18(5), 1895–1915. <https://doi.org/10.5194/hess-18-1895-2014>
- Giroto, M., De Lannoy, G. J. M., Reichle, R. H., Rodell, M., Draper, C., Bhanja, S. N., & Mukherjee, A. (2017). Benefits and pitfalls of grace data assimilation: A case study of terrestrial water storage depletion in India. *Geophysical Research Letters*, 44(9), 4107–4115. <https://doi.org/10.1002/2017GL072994>
- Global Runoff Data Center (GRDC). (2021). Bundesanstalt für Gewässerkunde (BFG). Retrieved from https://www.bafg.de/GRDC/EN/Home/homepage_node.html
- Gleeson, T., Wagener, T., Döll, P., Zipper, S. C., West, C., Wada, Y., et al. (2021). GMD perspective: The quest to improve the evaluation of groundwater representation in continental- to global-scale models. *Geoscientific Model Development*, 14(12), 7545–7571. <https://doi.org/10.5194/gmd-14-7545-2021>

- Gupta, H. V., Kling, H., Yilmaz, K. K., & Martinez, G. F. (2009). Decomposition of the mean squared error and NSE performance criteria: Implications for improving hydrological modelling. *Journal of Hydrology*, 377(1), 80–91. <https://doi.org/10.1016/j.jhydrol.2009.08.003>
- Healy, R. W., & Cook, P. G. (2002). Using groundwater levels to estimate recharge. *Hydrogeology Journal*, 10(1), 91–109. <https://doi.org/10.1007/s10404-001-0178-0>
- Hrachowitz, M., Fovet, O., Ruiz, L., Euser, T., Gharari, S., Nijzink, R., et al. (2014). Process consistency in models: The importance of system signatures, expert knowledge, and process complexity. *Water Resources Research*, 50(9), 7445–7469. <https://doi.org/10.1002/2014WR015484>
- ICOS RI. (2021). *Ecosystem final quality (I2) product in etc-archive format - Release 2021-1 (version 1.0)*. ICOS ERIC - Carbon Portal. <https://doi.org/10.18160/FZMY-PG92>
- International Groundwater Resources Assessment Center (IGRAC). (2021). Retrieved from <https://ggis.un-igrac.org/view/ggmn/>
- Janssen, G., van Walsum, P., America, I., Pouwels, J., Hunink, J., Vermeulen, P., et al. (2020). Veranderingssrapport LHM 4.1: Beheer en onderhoud van de landelijke toepassing van het NHI. Deltares rapport 11205261-000-BGS-0001. Retrieved from https://www.nhi.nl/nl/index.php/download_file/view/371/354/
- Jiménez-Rodríguez, C. D., Sulis, M., & Schymanski, S. (2022). Exploring the role of bedrock representation on plant transpiration response during dry periods at four forested sites in Europe. *Biogeosciences*, 19(14), 3395–3423. <https://doi.org/10.5194/bg-19-3395-2022>
- Jung, M., Reichstein, M., & Bondeau, A. (2009). Towards global empirical upscaling of FLUXNET eddy covariance observations: Validation of a model tree ensemble approach using a biosphere model. *Biogeosciences*, 6(10), 2001–2013. <https://doi.org/10.5194/bg-6-2001-2009>
- Kalma, J., McVicar, T., & McCabe, M. (2008). Estimating land surface evaporation: A review of methods using remotely sensed surface temperature data. *Surveys in Geophysics*, 29(4–5), 421–469. <https://doi.org/10.1007/s10712-008-9037-z>
- Keune, J., Gasper, F., Goergen, K., Hense, A., Shrestha, P., Sulis, M., & Kollet, S. (2016). Studying the influence of groundwater representations on land surface-atmosphere feedbacks during the European heat wave in 2003. *Journal of Geophysical Research: Atmospheres*, 121(22), 13301–13325. <https://doi.org/10.1002/2016JD025426>
- Knox, S. H., Jackson, R. B., Poulter, B., McNicol, G., Fluet-Chouinard, E., Zhang, Z., et al. (2019). FLUXNET-CH₄ synthesis activity: Objectives, observations, and future directions. *Bulletin of the American Meteorological Society*, 100(12), 2607–2632. <https://doi.org/10.1175/BAMS-D-18-0268.1>
- Kollet, S. J., & Maxwell, R. M. (2008). Capturing the influence of groundwater dynamics on land surface processes using an integrated, distributed watershed model. *Water Resources Research*, 44(2), W02402. <https://doi.org/10.1029/2007WR006004>
- Konapala, G., Mishra, A. K., Wada, Y., & Mann, M. E. (2020). Climate change will affect global water availability through compounding changes in seasonal precipitation and evaporation. *Nature Communications*, 11(3044), 3044. <https://doi.org/10.1038/s41467-020-16757-w>
- Koppa, A., Alam, S., Miralles, D. G., & Gebremichael, M. (2021). Budyko-based long-term water and energy balance closure in global watersheds from earth observations. *Water Resources Research*, 57(5), e2020WR028658. <https://doi.org/10.1029/2020WR028658>
- Koppa, A., Rains, D., Hulsman, P., Poyatos, R., & Miralles, D. G. (2022). A deep learning-based hybrid model of global terrestrial evaporation. *Nature Communications*, 13(1912), 1912. <https://doi.org/10.1038/s41467-022-29543-7>
- Krakauer, N., Li, H., & Fan, Y. (2014). Groundwater flow across spatial scales: Importance for climate modeling. *Environmental Research Letters*, 9(3), 034003. <https://doi.org/10.1088/1748-9326/9/3/034003>
- Kuffour, B. N. O., Engdahl, N. B., Woodward, C. S., Condon, L. E., Kollet, S., & Maxwell, R. M. (2020). Simulating coupled surface–subsurface flows with ParFlow v3.5.0: Capabilities, applications, and ongoing development of an open-source, massively parallel, integrated hydrologic model. *Geoscientific Model Development*, 13(3), 1373–1397. <https://doi.org/10.5194/gmd-13-1373-2020>
- Laio, F., Tamea, S., Ridolfi, L., D'Odorico, P., & Rodriguez-Iturbe, I. (2009). Ecohydrology of groundwater-dependent ecosystems: 1. Stochastic water table dynamics. *Water Resources Research*, 45(5). <https://doi.org/10.1029/2008WR007292>
- Lam, A., Karssenberg, D., van den Hurk, B. J. J. M., & Bierkens, M. F. P. (2011). Spatial and temporal connections in groundwater contribution to evaporation. *Hydrology and Earth System Sciences*, 15(8), 2621–2630. <https://doi.org/10.5194/hess-15-2621-2011>
- Landerer, F. W., & Swenson, S. C. (2012). Accuracy of scaled grc terrestrial water storage estimates. *Water Resources Research*, 48(4). <https://doi.org/10.1029/2011WR011453>
- Langevin, C., Hughes, J., Banta, E., Provost, A., Niswonger, R., & Panday, S. (2017). *MODFLOW 6 modular hydrologic model*. U.S. Geological Survey Software. <https://doi.org/10.5066/F76Q1VQV>
- Lawrence, D. M., Fisher, R. A., Koven, C. D., Oleson, K. W., Swenson, S. C., Bonan, G., et al. (2019). The Community Land Model Version 5: Description of new features, benchmarking, and impact of forcing uncertainty. *Journal of Advances in Modeling Earth Systems*, 11(12), 4245–4287. <https://doi.org/10.1029/2018MS001583>
- Liu, T., Liu, L., Luo, Y., & Lai, J. (2015). Simulation of groundwater evaporation and groundwater depth using swat in the irrigation district with shallow water table. *Environmental Earth Sciences*, 74(1), 315–324. <https://doi.org/10.1007/s12665-015-4034-2>
- Liu, T., & Luo, Y. (2012). An empirical approach simulating evapotranspiration from groundwater under different soil water conditions. *Environmental Earth Sciences*, 67(5), 1345–1355. <https://doi.org/10.1007/s12665-012-1577-3>
- Loew, A., Peng, J., & Borsche, M. (2016). High-resolution land surface fluxes from satellite and reanalysis data (HOLAPS v1.0): Evaluation and uncertainty assessment. *Geoscientific Model Development*, 9(7), 2499–2532. <https://doi.org/10.5194/gmd-9-2499-2016>
- Lovato, T., Peano, D., Butenschön, M., Matera, S., Iovino, D., Scoccimarro, E., et al. (2022). CMIP6 simulations with the CMCC earth system model (CMCC-ESM2). *Journal of Advances in Modeling Earth Systems*, 14(3), e2021MS002814. <https://doi.org/10.1029/2021MS002814>
- Lv, M., Xu, Z., Yang, Z.-L., Lu, H., & Lv, M. (2021). A comprehensive review of specific yield in land surface and groundwater studies. *Journal of Advances in Modeling Earth Systems*, 13(2), e2020MS002270. <https://doi.org/10.1029/2020MS002270>
- Mallick, K., Jarvis, A. J., Boegh, E., Fisher, J. B., Drewry, D. T., Tu, K. P., et al. (2014). A surface temperature initiated closure (STIC) for surface energy balance fluxes. *Remote Sensing of Environment*, 141, 243–261. <https://doi.org/10.1016/j.rse.2013.10.022>
- Martens, B., Miralles, D. G., Lievens, H., van der Schalie, R., de Jeu, R. A. M., Fernández-Prieto, D., et al. (2017). GLEAM v3: Satellite-based land evaporation and root-zone soil moisture. *Geoscientific Model Development*, 10(5), 1903–1925. <https://doi.org/10.5194/gmd-10-1903-2017>
- Martens, B., Schumacher, D. L., Wouters, H., Muñoz Sabater, J., Verhoest, N. E. C., & Miralles, D. G. (2020). Evaluating the land-surface energy partitioning in ERA5. *Geoscientific Model Development*, 13(9), 4159–4181. <https://doi.org/10.5194/gmd-13-4159-2020>
- Maxwell, R., & Condon, L. (2016). Connections between groundwater flow and transpiration partitioning. *Science*, 353(6297), 377–380. <https://doi.org/10.1126/science.aaf7891>
- Maxwell, R., & Miller, N. (2005). Development of a coupled land surface and groundwater model. *Journal of Hydrometeorology*, 6(3), 233–247. <https://doi.org/10.1175/JHM422.1>
- Mccormick, E. L., Dralle, D. N., Hahm, W. J., Tune, A. K., Schmidt, L. M., Chadwick, K. D., & Rempe, D. M. (2021). Widespread woody plant use of water stored in bedrock. *Nature*, 597(7875), 225–229. <https://doi.org/10.1038/s41586-021-03761-3>
- Miguez-Macho, G., & Fan, Y. (2021). Spatiotemporal origin of soil water taken up by vegetation. *Nature*, 598(7882), 624–628. <https://doi.org/10.1038/s41586-021-03958-6>

- Miralles, D. G., Holmes, T. R. H., De Jeu, R. A. M., Gash, J. H., Meesters, A. G. C. A., & Dolman, A. J. (2011). Global land-surface evaporation estimated from satellite-based observations. *Hydrology and Earth System Sciences*, 15(2), 453–469. <https://doi.org/10.5194/hess-15-453-2011>
- Moesinger, L., Dorigo, W., de Jeu, R., van der Schalie, R., Scanlon, T., Teubner, I., & Forkel, M. (2020). The global long-term microwave vegetation optical depth climate archive (VODCA). *Earth System Science Data*, 12(1), 177–196. <https://doi.org/10.5194/essd-12-177-2020>
- Müller Schmied, H., Cáceres, D., Eisner, S., Flörke, M., Herbert, C., Niemann, C., et al. (2021). The global water resources and use model WaterGAP v2.2d: Model description and evaluation. *Geoscientific Model Development*, 14(2), 1037–1079. <https://doi.org/10.5194/gmd-14-1037-2021>
- Niu, G.-Y., Yang, Z.-L., Dickinson, R. E., Gulden, L. E., & Su, H. (2007). Development of a simple groundwater model for use in climate models and evaluation with gravity recovery and climate experiment data. *Journal of Geophysical Research*, 112(D7), D07103. <https://doi.org/10.1029/2006JD007522>
- Oki, T., & Kanae, S. (2006). Global hydrological cycles and world water resources. *Science*, 313(5790), 1068–1072. <https://doi.org/10.1126/science.1128845>
- Orellana, F., Verma, P., Loheide, S. P., II, & Daly, E. (2012). Monitoring and modeling water-vegetation interactions in groundwater-dependent ecosystems. *Reviews of Geophysics*, 50(3), RG3003. <https://doi.org/10.1029/2011RG000383>
- Pastorello, G., Trotta, C., Canfora, E., Chu, H., Christianson, D., Cheah, Y.-W., et al. (2020). The FLUXNET2015 dataset and the ONEFlux processing pipeline for eddy covariance data. *Scientific Data*, 7(1), 225. <https://doi.org/10.1038/s41597-020-0534-3>
- Priestley, C. H. B., & Taylor, R. J. (1972). On the assessment of surface heat flux and evaporation using large-scale parameters. *Monthly Weather Review*, 100(2), 81–92. [https://doi.org/10.1175/1520-0493\(1972\)100<0081:OTAOSH>2.3.CO;2](https://doi.org/10.1175/1520-0493(1972)100<0081:OTAOSH>2.3.CO;2)
- Reinecke, R., Wachholz, A., Mehl, S., Foglia, L., Niemann, C., & Döll, P. (2020). Importance of spatial resolution in global groundwater modeling. *Groundwater*, 58(3), 363–376. <https://doi.org/10.1111/gwat.12996>
- Rempe, D. M., & Dietrich, W. E. (2018). Direct observations of rock moisture, a hidden component of the hydrologic cycle. *Proceedings of the National Academy of Sciences*, 115(11), 2664–2669. <https://doi.org/10.1073/pnas.1800141115>
- Samaniego, L., Kumar, R., & Attinger, S. (2010). Multiscale parameter regionalization of a grid-based hydrologic model at the mesoscale. *Water Resources Research*, 46(5), W05523. <https://doi.org/10.1029/2008WR007327>
- Scholes, R., & Brown de Colstoun, E. (2011). *ISLSCP II global gridded soil characteristics*. ORNL Distributed Active Archive Center. <https://doi.org/10.3334/ORNLDAAC/1004>
- Su, Z. (2002). The surface energy balance system (SEBS) for estimation of turbulent heat fluxes. *Hydrology and Earth System Sciences*, 6(1), 85–100. <https://doi.org/10.5194/hess-6-85-2002>
- Sulis, M., Couvreur, V., Keune, J., Cai, G., Trebs, I., Junk, J., et al. (2019). Incorporating a root water uptake model based on the hydraulic architecture approach in terrestrial systems simulations. *Agricultural and Forest Meteorology*, 269, 28–45. <https://doi.org/10.1016/j.agrformet.2019.01.034>
- Sulis, M., Williams, J., Shrestha, P., Diederich, M., Simmer, C., Kollet, S., & Maxwell, R. (2017). Coupling groundwater, vegetation, and atmospheric processes: A comparison of two integrated models. *Journal of Hydrometeorology*, 18(5), 1489–1511. <https://doi.org/10.1175/JHM-D-16-0159.1>
- Sutanudjaja, E. H., van Beek, R., Wanders, N., Wada, Y., Bosmans, J. H. C., Drost, N., et al. (2018). PCR-GLOBWB 2: A 5 arcmin global hydrological and water resources model. *Geoscientific Model Development*, 11(6), 2429–2453. <https://doi.org/10.5194/gmd-11-2429-2018>
- Swenson, S., & Wahr, J. (2006). Post-processing removal of correlated errors in grace data. *Geophysical Research Letters*, 33(8), L08402. <https://doi.org/10.1029/2005GL025285>
- Takala, M., Luojus, K., Pulliaiainen, J., Derksen, C., Lemmettyinen, J., Kärnä, J.-P., et al. (2011). Estimating northern hemisphere snow water equivalent for climate research through assimilation of space-borne radiometer data and ground-based measurements. *Remote Sensing of Environment*, 115(12), 3517–3529. <https://doi.org/10.1016/j.rse.2011.08.014>
- Taylor, R. G., Scanlon, B., Döll, P., Rodell, M., van Beek, R., Wada, Y., et al. (2013). Ground water and climate change. *Nature Climate Change*, 3(4), 322–329. <https://doi.org/10.1038/nclimate1744>
- Tfawalat, C., van Rensburg, L., & Bello, Z. (2021). Groundwater contribution to transpiration of trees under wet and dry soil conditions. *Irrigation and Drainage*, 70(1), 42–51. <https://doi.org/10.1002/ird.2533>
- Tian, W., Li, X., Cheng, G.-D., Wang, X.-S., & Hu, B. X. (2012). Coupling a groundwater model with a land surface model to improve water and energy cycle simulation. *Hydrology and Earth System Sciences*, 16(12), 4707–4723. <https://doi.org/10.5194/hess-16-4707-2012>
- Trenberth, K. E., Fusilero, J., & Kiehl, J. (2009). Earth's global energy budget. *American Meteorological Society*, 90(90), 311–323. <https://doi.org/10.1175/2008BAMS2634.1>
- Trenberth, K. E., Smith, L., Qian, T., Dai, A., & Fusilero, J. (2007). Estimates of the global water budget and its annual cycle using observational and model data. *Journal of Hydrometeorology*, 8(4), 758–769. <https://doi.org/10.1175/JHM600.1>
- van der Ent, R. J., Savenije, H. H. G., Schaefli, B., & Steele-Dunne, S. C. (2010). Origin and fate of atmospheric moisture over continents. *Water Resources Research*, 46(9), W09525. <https://doi.org/10.1029/2010WR009127>
- Vicente-Serrano, S. M., Beguería, S., & López-Moreno, J. I. (2010). A multiscale drought index sensitive to global warming: The standardized precipitation evapotranspiration index. *Journal of Climate*, 23(7), 1696–1718. <https://doi.org/10.1175/2009JCLI2909.1>
- Wielicki, B. A., Barkstrom, B. R., Harrison, E. F., Lee, R. B., Smith, G. L., & Cooper, J. E. (1996). Clouds and the Earth's radiant energy system (CERES): An earth observing system experiment. *Bulletin of the American Meteorological Society*, 77(5), 853–868. [https://doi.org/10.1175/1520-0477\(1996\)077<0853:CATERE>2.0.CO;2](https://doi.org/10.1175/1520-0477(1996)077<0853:CATERE>2.0.CO;2)
- Yeh, P.-F., & Eltahir, E. (2005). Representation of water table dynamics in a land surface scheme. Part I: Model development. *Journal of Climate*, 18(12), 1861–1880. <https://doi.org/10.1175/JCLI3330.1>
- Yoshida, T., Hanasaki, N., Nishina, K., Boulange, J., Okada, M., & Troch, P. A. (2022). Inference of parameters for a global hydrological model: Identifiability and predictive uncertainties of climate-based parameters. *Water Resources Research*, 58(2), e2021WR030660. <https://doi.org/10.1029/2021WR030660>
- Zhang, J., Bai, Y., Yan, H., Guo, H., Yang, S., & Wang, J. (2020). Linking observation, modelling and satellite-based estimation of global land evapotranspiration. *Big Earth Data*, 4(2), 94–127. <https://doi.org/10.1080/20964471.2020.1743612>
- Zhang, K., Kimball, J. S., & Running, S. W. (2016). A review of remote sensing based actual evapotranspiration estimation. *WIREs Water*, 3(6), 834–853. <https://doi.org/10.1002/wat2.1168>